



HAL
open science

Hexanuclear $Zn^{II}_4Fe^{III}_2$ and $Zn^{II}_4Cr^{III}_2$ complexes from the use of potentially tetradentate NOO'O" Schiff-base ligands

Konstantinos N Pantelis, Sotiris G Skiadas, Zoi G Lada, Rodolphe Clérac, Yiannis Sanakis, Pierre Dechambenoit, Spyros P Perlepes

► **To cite this version:**

Konstantinos N Pantelis, Sotiris G Skiadas, Zoi G Lada, Rodolphe Clérac, Yiannis Sanakis, et al.. Hexanuclear $Zn^{II}_4Fe^{III}_2$ and $Zn^{II}_4Cr^{III}_2$ complexes from the use of potentially tetradentate NOO'O" Schiff-base ligands. *New Journal of Chemistry*, 2024, 48 (25), pp.11221-11232. 10.1039/d4nj02030h . hal-04637191

HAL Id: hal-04637191

<https://hal.science/hal-04637191v1>

Submitted on 5 Jul 2024

HAL is a multi-disciplinary open access archive for the deposit and dissemination of scientific research documents, whether they are published or not. The documents may come from teaching and research institutions in France or abroad, or from public or private research centers.

L'archive ouverte pluridisciplinaire **HAL**, est destinée au dépôt et à la diffusion de documents scientifiques de niveau recherche, publiés ou non, émanant des établissements d'enseignement et de recherche français ou étrangers, des laboratoires publics ou privés.

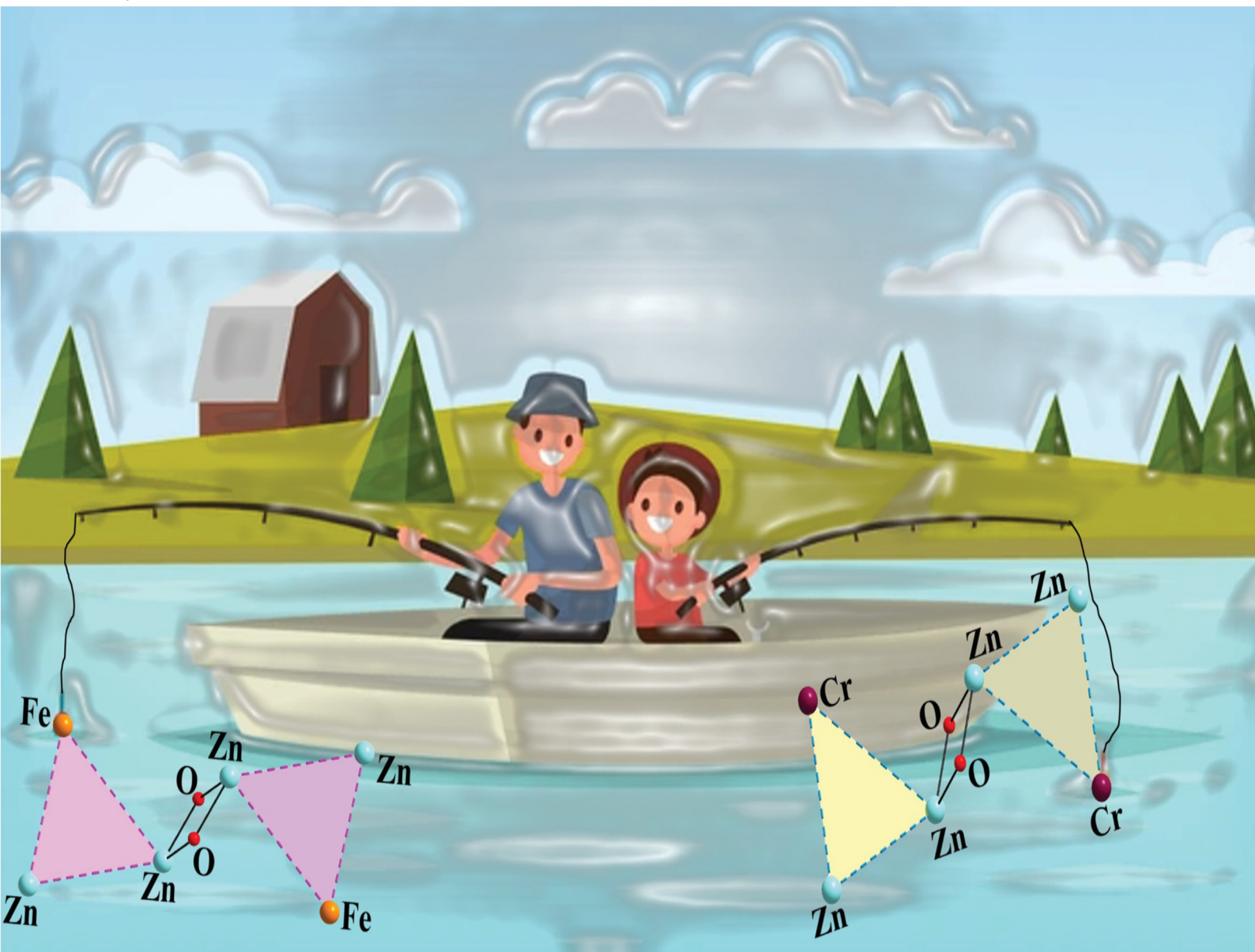


Distributed under a Creative Commons Attribution - NonCommercial 4.0 International License

NJC

New Journal of Chemistry
rsc.li/njc

A journal for new directions in chemistry



ISSN 1144-0546

PAPER

Yiannis Sanakis, Pierre Dechambenoit, Spyros P. Perlepes *et al.*
Hexanuclear $\{Zn_4Fe_2\}$ and $\{Zn_4Cr_2\}$ complexes from the use
of potentially tetradentate NOO'O" Schiff-base ligands


 Cite this: *New J. Chem.*, 2024, 48, 11221

Hexanuclear $\{Zn_4^II Fe_2^III\}$ and $\{Zn_4^II Cr_2^III\}$ complexes from the use of potentially tetradentate NOO'O' Schiff-base ligands†‡

 Konstantinos N. Pantelis,^a Sotiris G. Skiadas,^{id}^a Zoi G. Lada,^{id}^b Rodolphe Clérac,^{id}^c Yiannis Sanakis,^{*d} Pierre Dechambenoit^{*c} and Spyros P. Perlepes^{id}^{*ab}

The use of *N*-(2-carboxyphenyl)salicylideneimine (saphHCOOH) and *N*-(4-chloro-carboxyphenyl)salicylideneimine (4ClSaphHCOOH) for the synthesis of hexanuclear $\{Zn_4^II M_2^III\}$ (*M* = Cr, Fe) complexes is described. $[Zn_4Fe_2(saphCOO)_6(NO_3)_2(EtOH)_2]$ (**1**), $[Zn_4Cr_2(saphCOO)_6(NO_3)_2(H_2O)_2]$ (**2**) and $[Zn_4Fe_2(4Cl-saphCOO)_6(NO_3)_2(EtOH)_2]$ (**3**), as $4CH_2Cl_2 \cdot 2EtOH$ (**1**, **3**) and $4MeCN \cdot 2EtOH$ (**2**) solvates, have been isolated and their structures have been determined by single-crystal X-ray crystallography. The three complexes are centrosymmetric and almost isostructural. The metal topology can be described as two isosceles triangles which are linked through phenolate oxygen atoms of two 3.2111 (Harris notation) $saphCOO^{2-}/4ClSaphCOO^{2-}$ ligands, each of which bridges exclusively three Zn^{II} atoms. Four 2.1111 ligands are also incorporated in the molecules, each bridging one M^{III} center and one Zn^{II} ion. The former is chelated with the $O_{phenolate}$, N_{imine} and one $O_{carboxylate}$ being the donor atoms (thus forming two 6-membered chelating rings with a common $M^{III}-N$ edge), while the latter is bound to the other carboxylate oxygen. The coordination spheres are of the types $\{FeO_4N_2\}/\{ZnO_4N\}/\{ZnO_5\}$ for **1** and **3**, and $\{CrO_4N_2\}/\{ZnO_4N\}/\{ZnO_4\}$ for **2**. Complexes **1–3** are the first heterometallic complexes (with any metals) based on saphHCOOH and 4ClSaphHCOOH, thus illustrating their ability for the preparation of mixed-metal molecular species. Interesting H-bonding patterns are present in the crystal structures. The IR and Raman spectra of the solid complexes are discussed in terms of the coordination modes of the ligands involved, while molar conductivity data and UV/VIS spectra in CH_2Cl_2 are also reported and interpreted. The δ and ΔE_Q ^{57}Fe -Mössbauer parameters of **1** and **3** at 300 and 80 K indicate isolated high-spin Fe^{III} centers. Variable-temperature (1.8–300 K) magnetic susceptibility data for **1–3** suggest a very weak exchange interaction between the M^{III} ions in agreement with their long distances (~ 9 Å) in the molecules.

 Received 1st May 2024,
 Accepted 28th May 2024

DOI: 10.1039/d4nj02030h

rsc.li/njc

^a Department of Chemistry, University of Patras, Patras 26504, Greece.

E-mail: perlepes@upatras.gr

^b Institute of Chemical Engineering Sciences (ICE-HT), Foundation for Research and Technology-Hellas (FORTH), Platani, P.O. Box 144, Patras 26504, Greece

^c Univ. Bordeaux, CNRS, CRPP, UMR 5031, F-33600 Pessac, France.

E-mail: pierre.dechambenoit@u-bordeaux.fr

^d Institute of Nanoscience and Nanotechnology, NCSR "Demokritos", Aghia Paraskevi Attikis 15310, Greece. E-mail: i.sanakis@inn.demokritos.gr

† Dedicated to Professor Mark Turnbull on the occasion of his retirement; a great inorganic chemist and magnetochemist, a precious friend.

 ‡ Electronic supplementary information (ESI) available: Crystallographic data (Table S1), structural plots (Fig. S1–S8), various spectra (Fig. S9–S14) and magnetic measurements plots (Fig. S15–S18). CCDC 2316071–2316073. For ESI and crystallographic data in CIF or other electronic format see DOI: <https://doi.org/10.1039/d4nj02030h>

Introduction

The field of mixed-metal, atom- or ion-based materials is receiving^{1–3} great attention of researchers working in solid-state chemistry and condensed-matter physics, for example in the area of multiferroics.² Molecular inorganic chemists are also interested in synthesizing and characterizing mixed-metal compounds. This general topic is stimulated by its relevance to several areas of bioinorganic chemistry,^{4,5} molecular nanomagnetism,^{6,7} catalysis,⁸ metallosupramolecular chemistry,⁹ porous complexes,¹⁰ quantum technology¹¹ and development of precursors for multifunctional materials.¹² Despite the recent explosive growth on complexes containing two different transition-metal ions,^{13,14} such complexes are significantly less reported in comparison to the plethora of 3d–4f species.^{15–20} With this in mind, we have initiated a project to examine the

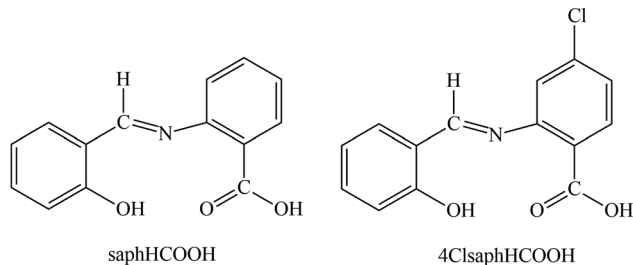


synthesis, structures and properties of heterometallic 3d–3d' complexes.

From a synthetic inorganic chemistry viewpoint, methods must be developed to combine two different 3d-metal ions. For some 3d-metal ion pairs, e.g. Fe^{III}–Ni^{II} and Fe^{III}–Cu^{II}, strategies can be used based on the HSAB model.^{15,21} For other pairs, e.g. the pairs Cr^{III}–Zn^{II} and Fe^{III}–Zn^{II} of the present work, this is not an easy task and often simply combining sources of the two different metal ions leads to complexes containing only one of them; thus success is many times results from several “try and see” exercises. It is obvious that this “self-assembly” process to prepare 3d–3d' metal complexes is heavily relied on the choice of the organic ligand.²²

Polydentate O,N-based Schiff bases are candidates for this goal. Even 160 years after their first synthesis by the Italian-German Hugo Schiff (1834–1915), these azomethine (–CH=N–) or imine (>C=N–) groups-containing molecules continue to surprise inorganic chemists because of their close relevance to a number of interdisciplinary research fields.^{23–25} Because of their logical modular synthesis that allows strict control over the nature of donor atoms, denticity, chelating and/or bridging function, as well as their adjustable electronic and steric features, polydentate Schiff bases have played a great role in the development of coordination chemistry after the second world war,²⁶ being also important for the preparation of heterometallic complexes.^{23–26} In a broader sense, formation of azomethines/imines is one of the types of reactions which define dynamic covalent chemistry (DCC), an approach which is used in the synthesis of complicated molecules and extended structures because of the inherent “proof-reading” and “error-checking” associated with these reversible processes.^{27,28}

An interesting group of the family of tetradentate Schiff-base ligands consists of molecules derived from the condensation of salicylaldehyde (or its derivatives) with 2-aminobenzoic acid (or its derivatives). Two members of this group have been employed in this work, namely *N*-(2-carboxylphenyl)salicylideneimine [the IUPAC name is {(2-hydroxyphenyl)methylidene}amino]benzoic acid] abbreviated as saphHCOOH, and *N*-(4-chloro-carboxylphenyl)salicylideneimine [the IUPAC name is 4-chloro-{(2-hydroxyphenyl)methylidene}amino]benzoic acid] abbreviated as 4ClsaphHCOOH; the two H atoms in the abbreviations denote the number of the ionizable protons. The structural formulas of the free neutral ligands are illustrated in Scheme 1. These molecules contain an ONO'O" donor set; deprotonation of the –COOH group or both the –COOH and –OH groups may favor coordination of the resulting anionic ligands to two or more same or different metal ions, thus resulting in dimers, polynuclear coordination complexes or polymers. Somewhat to our surprise, the coordination chemistry of saphHCOO[–] and saphCOO^{2–} has been exclusively limited to homometallic complexes (selected literature is given in ref. 29–33); no heterometallic compounds have been structurally characterized. The metal chemistry of 4ClsaphHCOOH is almost completely unexplored (by contrast with its 5-chloro analogue for which interesting homometallic complexes have been reported),^{34,35} the only structurally characterized complex being



Scheme 1 The structural formula of the two potentially tetradentate ONO'O" Schiff-base ligands used in the present work and their abbreviations. The single-crystal X-ray structure of saphHCOOH³⁸ reveals that the compound exists in the solid state as an intermediate form between the phenol-imine (illustrated in this scheme) and quinoid tautomers.

[Cu(4ClsaphCOO)(phen)], where phen is the chelating ancillary ligand 1,10-phenanthroline.^{36,37}

In this work, we describe our efforts to prepare Zn^{II}–Fe^{III} and Zn^{II}–Cr^{III} compounds based on saphHCOOH and 4ClsaphHCOOH. Zn^{II}–Fe^{III} complexes are interesting to the scientific community because: (i) the heterodinuclear {Zn^{II}Fe^{III}} unit has been recognized at the active sites of purple acid phosphatase and human calcineurin that facilitate the hydrolysis of phosphodiester into phosphomonoesters, and several complexes have been reported as structural and functional models of these enzymes;^{39,40} (ii) the ternary zinc ferrite, Zn^{II}Fe^{III}O₄, has been recognized as one of the promising lithium ion batteries anode substitutes⁴¹ and molecular analogues of this mixed-metal oxide are highly desirable; (iii) 3D porous frameworks containing Zn^{II} and Fe^{III} exhibit high CO₂/N₂ and CO₂/CH₄ selectivity;⁴² (iv) formal reduction of Fe^{III} complexes containing redox-active pincer ligands leads to “metalloligands” of Fe^{II} which allow the construction of iron–zinc complexes with interesting redox and magnetic properties;⁴³ and (v) Zn^{II} is an ideal diamagnetic substitute for Co^{II} in polynuclear Co^{II}/Fe^{III} complexes allowing for the in-depth understanding of the iron(III)–iron(III) magnetic interactions in such complexes. Zn^{II}–Cr^{III} complexes attract the interest of the inorganic chemistry community because – among others –: (i) diamagnetic Zn^{II} “metalloligands” can be used in the study of the presence of long-range Cr^{III}–Cr^{III} exchange interactions even if the distance between the paramagnetic metal ions is as long as ~7 Å;⁴⁴ (ii) the simultaneous presence of the two metal ions have resulted in a new trinodal metal–organic material platform comprised of simple and inexpensive triangular, tetrahedral and trigonal-prismatic molecular building blocks,⁴⁵ leading to molecular materials with chemical stability (organic solvents, water and bases) and high uptake of CO₂ and H₂. These properties are desirable in the context of the cost/performance ratio that is needed to develop metal–organic materials for applications; (iii) heterometallic Anderson-type {Zn₅^{II}Cr₂^{III}} “wheels” help in the in-depth study of substitutional disorder in the positions of the Cr^{III} and Zn^{II} ions around the outside ring;⁴⁶ (iv) heterometallic rings based on generic {(Zn_x^{II}Cr_y^{III})} formulas (*x*, *y* are integer numbers) exhibit exciting structural and physical properties, and they have been



proposed for various applications⁴⁷ including quantum information processing⁴⁸ and magnetic refrigeration;⁴⁹ and (v) doping of cyclic $\{\text{Zn}^{\text{II}}\text{Cr}^{\text{III}}\}$ molecular nanomagnets into diamagnetic and isostructural hosts allows pulsed X-band EPR studies (including relaxation and nutation experiments on the $S = 3/2$ ground state), the doping without scrambling of the Cr^{III} and Zn^{II} ions being aided by the kinetic inertness of the former.⁵⁰

This work can also be considered as a continuation of the interest of our groups in various aspects of the coordination chemistry of N,O-based Schiff bases.^{22,30,33,51–55}

Experimental section

Materials and instrumentation

All manipulations were performed under aerobic conditions using reagents and solvents (Sigma-Aldrich) as received. The free ligands saphHCOOH^{29,32,56} and 4ClisaphHCOOH^{36,37,57} were synthesized as described in the literature; their purity was checked by ¹H NMR spectroscopy in DMSO-*d*₆. C, H and N microanalyses were conducted by the Instrumental Analysis Laboratory of the University of Patras using a Carlo-Erba analyzer, model EA 1108. FT-IR spectra (4000–400 cm⁻¹) were recorded using a PerkinElmer 16PC spectrometer with samples prepared as KBr (spectroscopic grade) pellets under pressure. Raman spectra were recorded on a T-64000 Jobin Yvon-Horiba micro-Raman setup utilized in a single-spectrograph configuration. The excitation wavelength was 514.5 nm emitted from a DPSS laser (Cobolt Fandango TMISO Laser, Norfolk, UK). The laser power on the samples was 1 mW. The backscattered radiation was collected from a single configuration of the monochromator after passing through an appropriate edge filter (LP02-633RU-25, Laser2000 Ltd, Huntingdon, Cambridgeshire, UK). The calibration of the instrument was achieved *via* the standard peak position of Si at 520.5 cm⁻¹. The spectral resolution was 5 cm⁻¹. UV/Vis spectra in solution were recorded on a Hitachi U-300 spectrometer. Conductivity measurements in CH₂Cl₂ were carried out at room temperature (22–24 °C) with a Metrohm-Herisau E-527 bridge and a cell of standard design; the concentration of the solutions was $\sim 10^{-3}$ M. ¹H NMR spectra in DMSO-*d*₆ (to check the purity of the free ligands) were run on a 600.13-MHz Bruker Avance DPX spectrometer. ⁵⁷Fe-Mössbauer spectra from powdered dried samples of the iron(III)-containing complexes were recorded using a constant-acceleration conventional spectrometer with a source of ⁵⁷Co (Rh matrix). Spectra in the 80–300 K range were obtained using a Janis cryostat. Isomer shift values (δ) are reported relative to the Fe foil at 293 K. Magnetic susceptibility and magnetization measurements were performed on a Quantum Design SQUID magnetometer MPMS-XL at temperatures between 1.8 and 300 K, and dc magnetic fields ranging from –7 to +7 T. The data were collected on polycrystalline samples suspended in mineral oil and introduced in a sealed polyethylene bag. Prior to the experiments, the field-dependent magnetization was measured at 100 K on each sample in order to detect the presence of any bulk ferromagnetic impurities; paramagnetic

or diamagnetic materials should exhibit a strictly linear dependence of magnetization that extrapolates to zero at zero dc field. The samples appeared to be free of any ferromagnetic impurities. The magnetic susceptibilities were corrected for the oil, the sample holder, and the intrinsic diamagnetic contributions.

Synthetic details

Synthesis of $[\text{Zn}_4\text{Fe}_2(\text{saphCOO})_6(\text{NO}_3)_2(\text{EtOH})_2]\cdot 4\text{CH}_2\text{Cl}_2\cdot 2\text{EtOH}$ (1- $4\text{CH}_2\text{Cl}_2\cdot 2\text{EtOH}$). Solid $\text{Zn}(\text{O}_2\text{CMe})_2\cdot 2\text{H}_2\text{O}$ (0.044 g, 0.20 mmol) was added to a yellow solution of saphHCOOH (0.048 g, 0.20 mmol) in EtOH/CH₂Cl₂ (20 mL, 1:1 v/v). To the resulting yellow suspension was added solid $\text{Fe}(\text{NO}_3)_3\cdot 9\text{H}_2\text{O}$ (0.040 g, 0.10 mmol). A dark red solution was obtained which was stirred for 1 h and then layered with Et₂O (5 mL). X-ray quality brown crystals of the product were precipitated within 11 d. The crystals were collected by filtration, washed with Et₂O (2 × 2 mL) and dried in a vacuum desiccator, first over silica gel and later over P₄O₁₀. The yield was *ca.* 60% (based on the ligand available). The sample was analyzed satisfactorily as lattice solvent-free (1). Anal. calcd for C₈₈H₆₆N₈O₂₆Zn₄Fe₂: C 52.20; H 3.29; N 5.53%. Found: C 52.46; H 3.27; N 5.39%. IR (KBr, cm⁻¹): 3422wb, 2925w, 1591s, 1544s, 1490m, 1469sh, 1447m, 1384s, 1295m, 1228w, 1185m, 1153m, 1126w, 1095w, 1040w, 923w, 875m, 850w, 795m, 760m, 714m, 687w, 648w, 604w, 560w, 523w, 461w, 417w. Selected Raman peaks (cm⁻¹): 1614s, 1587s, 1534m, 1458w, 1410w, 1361w, 1340m, 1310w, 1272w, 1251w, 1186m, 1164w, 613s, 563m. UV/Vis (CH₂Cl₂, nm): 230sb, 258sh, 285sh, 380mb, 405mb, 510wb, 585wb. Λ_{M} (CH₂Cl₂, 10⁻³ M, 23 °C) = 4 S cm² mol⁻¹. ⁵⁷Fe-Mössbauer (mm s⁻¹): $\delta = \sim 0.35$ and $\Delta E_{\text{Q}} = \sim 0.6$ at room temperature.

Synthesis of $[\text{Zn}_4\text{Cr}_2(\text{saphCOO})_6(\text{NO}_3)_2(\text{H}_2\text{O})_2]\cdot 4\text{MeCN}\cdot 2\text{EtOH}$ (2- $4\text{MeCN}\cdot 2\text{EtOH}$). Solid $\text{Zn}(\text{O}_2\text{CMe})_2\cdot 2\text{H}_2\text{O}$ (0.044 g, 0.20 mmol) was added to a stirred yellow solution of saphHCOOH (0.048 g, 0.20 mmol) in EtOH/MeCN (10 mL, 1:1 v/v). To the resulting yellow suspension was added solid $\text{Cr}(\text{NO}_3)_3\cdot 9\text{H}_2\text{O}$ (0.040 g, 0.10 mmol). An olive green solution was obtained, which was stirred under reflux for 2 h. No noticeable color change took place. The solution was layered with Et₂O (4 mL) and reddish green X-ray quality crystals of the product were precipitated in a period of 5 d. The crystals were collected by filtration, washed with Et₂O and dried in a vacuum desiccator, first over silica gel and later over anhydrous CaCl₂. The yield was *ca.* 50% (based on the ligand available). The sample was analyzed satisfactorily as lattice solvent-free, *i.e.* as 2. Anal. calcd for C₈₄H₅₈N₈O₂₆Zn₄Cr₂: C 51.44; H 2.99; N 5.71%. Found: C 51.78; H 2.87; N 5.87%. IR (KBr, cm⁻¹): 3482mb, 1594s, 1552m, 1467sh, 1449m, 1384s, 1293m, 1230w, 1188w, 1152w, 1126w, 1095w, 1042w, 926w, 878w, 857w, 797w, 761m, 714w, 690w, 616w, 538w, 462w, 441w. Selected Raman peaks (cm⁻¹): 1630m, 1587s, 1545m, 1473m, 1442s, 1308w, 1275w, 1186m, 1156w, 624m, 461w. UV/Vis (CH₂Cl₂, nm): 225mb, 240mb, 280wb, 325wb, 420wb, 522wb, 583wb. Λ_{M} (CH₂Cl₂, 10⁻³ M, 23 °C) = 2 S cm² mol⁻¹.

Synthesis of $[\text{Zn}_4\text{Fe}_2(4\text{ClisaphCOO})_6(\text{NO}_3)_2(\text{EtOH})_2]\cdot 4\text{CH}_2\text{Cl}_2\cdot 2\text{EtOH}$ (3- $4\text{CH}_2\text{Cl}_2\cdot 2\text{EtOH}$). This complex was prepared in the exactly same manner (*i.e.* equivalents of reactants, solvents, concentration, crystallization method) as compound 1-



4CH₂Cl₂·2EtOH, but by using 4Cl_ssaphHCOOH (0.055 g, 0.20 mmol) in place of saphHCOOH. After 4 d reddish brown crystals of the product appeared, which were collected by filtration, washed with Et₂O (2 × 2 mL) and dried in a vacuum desiccator over P₄O₁₀. The yield was ~40% (based on the ligand available). The sample was analyzed satisfactorily as lattice solvent-free (3). Anal. calcd for C₈₈H₆₀N₈O₂₆Cl₆Zn₄Fe₂: C 47.36; H 2.72; N 5.02%. Found: C 47.19; H 2.86; N 4.89%. IR (KBr, cm⁻¹): 3480sb, 1587s, 1541s, 1486w, 1469w, 1443m, 1401m, 1384m, 1292s, 1225w, 1185m, 1150m, 1112w, 1085w, 1027w, 982w, 938s, 904s, 864m, 786m, 764s, 707w, 632w, 603w, 513w, 474w, 419w. Selected Raman peaks (cm⁻¹): 1616s, 1583m, 1534m, 1442m, 1371m, 1346m, 1317m, 1183m, 610s, 564m. UV/Vis (CH₂Cl₂, nm): 230sb, 290sh, 375mb, 410wb, 520wb, 590wb. A_M (CH₂Cl₂, 10⁻³ M, 24 °C) = 1 S cm² mol⁻¹. ⁵⁷Fe-Mössbauer (mm s⁻¹): δ = 0.38 mm s⁻¹ and ΔE_Q = 0.45 at room temperature.

Single-crystal X-ray crystallography

Crystals of the complexes were taken directly from the mother liquor. Crystallographic data were collected with a Bruker APEX II Quasar diffractometer, equipped with a graphite monochromator centered on the path of Mo K α radiation. The crystals were coated with Cargille™ NHV immersion oil and mounted on a fiber loop, followed by data collection at 120 K. The program SAINT was used to integrate the data, which were therefore corrected using SADABS.⁵⁸ The structures were solved using SHELXT⁵⁹ and refined by a full-matrix least-squares technique on F² using SHELXL-2019.⁶⁰ All non-H atoms were refined with anisotropic displacement parameters, whereas H atoms were assigned to ideal positions and refined isotropically using a suitable riding model, except those on the O atom of coordinated EtOH or H₂O molecules, which were located on the difference density map and introduced using DFIX constraints.

The crystals of 1·4CH₂Cl₂·2EtOH and 3·4CH₂Cl₂·2EtOH are small and weakly diffracting. Therefore, the data were cut at 0.90 and 1.00 Å, respectively, as there is no diffraction above and R_{int} becomes larger. The result is quite low θ_{\max} values and data/parameters ratios.

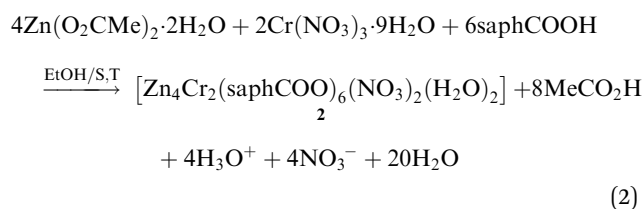
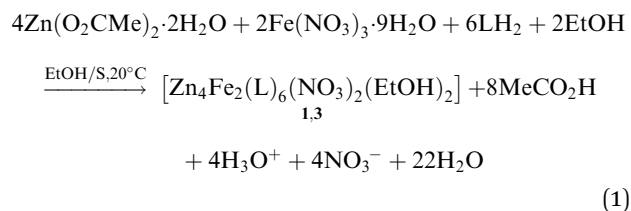
The CIF files have been deposited at the Cambridge Crystallographic Data Center as supplementary publication with the deposition numbers 2316071–2316073.† Crystallographic data are summarized in Table S1 (ESI†).

Results and discussion

Synthetic comments

As stated in “Introduction”, our goal was to prepare heterometallic Zn^{II}–Fe^{III} and Zn^{II}–Cr^{III} complexes based on saphHCOOH and 4Cl_ssaphHCOOH. Several synthetic parameters were investigated, such as the source of the two metal ions (nitrate, acetate, halide, perchlorate), the solvent, the concentration, the molar ratio of the reactants, the absence/presence of external bases (LiOH, NaOMe, Et₃N), the reaction time, the temperature,

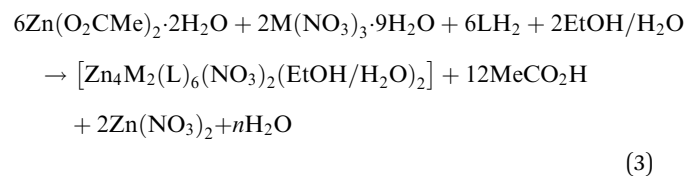
the pressure (*i.e.* solvothermal techniques) and the crystallization techniques, before arriving at the optimized processes described in the Experimental section. The best choice of the metal sources for obtaining single crystals of the products were Zn(O₂CMe)₂·2H₂O, and the nitrate “salts” of Fe^{III} and Cr^{III}. The ideal solvents proved to be EtOH/CH₂Cl₂ for the Zn^{II}/Fe^{III} complexes and MeCN/EtOH for the Zn^{II}/Cr^{III} compound. Elevated temperatures (*i.e.* refluxing conditions) were necessary to overcome the kinetic inertness of the 3d³ Cr^{III} ion. Assuming that the hexanuclear complexes are the only products from their respective reaction mixtures, the formation of 1–3 can be summarized by eqn (1) and (2), where LH₂ is saphHCOOH or 4Cl_ssaphHCOOH, and S is CH₂Cl₂ for 1, 3 and MeCN for 2:



Few synthetic points deserve comments: (i) small changes in the reactants' ratio do not affect the product identity. (ii) Heterometallic complexes containing the singly deprotonated saphHCOO⁻ and 4Cl_ssaphHCOO⁻ ligands could not be prepared. (iii) A procedure similar to that described for 2, but using 4Cl_ssaphHCOOH instead of saphHCOOH, gave a green powder whose analytical data are consistent with the formulation [Zn₄Cr₂(4Cl_ssaphCOO)₆(NO₃)₂(H₂O)₂]:xsolvents; in addition, the IR spectrum of this powder is similar to that of 2. However, since we could not obtain single crystals of this product, its characterization was not pursued further; and (iv) looking at the stoichiometric chemical eqn (1) and (2) we see that dilute HNO₃ (strong acid) is also produced, which might decompose 1–3, *e.g.* by singly protonating the coordinated dianionic ligands. We believe that the released protons are neutralized by the MeCO₂⁻ ions that are present in excess in the reaction mixture. The stoichiometric MeCO₂⁻:saphHCOOH/4Cl_ssaphHCOOH molar ratio indicated by eqn (1) and (2) is 8:6, whereas the experimental one is 2:1 (*i.e.* 12:6); this means that the acetates are in excess acting as additional effective proton acceptors. In support of this viewpoint, the complexes can not be isolated using an 1:1.5 Zn(O₂CMe)₂·2H₂O:LH₂ (*i.e.* MeCO₂⁻:LH₂ = 4:6) ratio. Thus, an alternative description of the actual processes, perhaps more correct, can be represented by eqn (3); in this equation M is Fe or Cr, LH₂ is saphHCOOH (for 1 and 2) or 4Cl_ssaphHCOOH (in the case of 3) and n = 30. If this is correct, Fe^{III} and Cr^{III} are in deficiency in the reaction mixtures and this is consistent with the moderate yields (*ca.* 50%) of the



reactions.



Description of structures

The structures of the three complexes have been determined by single-crystal X-ray crystallography. Selected interatomic distances and bond angles are listed in Tables 1 and 2. Various structural plots are shown in Fig. 1–7 and Fig. S1–S8 (ESI[†]). Further details can be found in the deposited CIFs. The molecular structures of the three complexes are very similar and thus only the structure of **1**·4CH₂Cl₂·2EtOH will be described in detail.

Complex **1**·4CH₂Cl₂·2EtOH crystallizes in the monoclinic space group *P*₂₁/*c*. Its structure consists of hexanuclear [Zn₄Fe₂-(saphCOO)₆(NO₃)₂(EtOH)₂] molecules, and lattice CH₂Cl₂ and EtOH molecules in an 1:4:2 ratio; the latter two will be not described here, but later in the context of the supramolecular interactions. The hexanuclear molecule possesses a crystallographically imposed inversion center, which is located at the midpoint of the Zn1···Zn1' vector. The metal topology can be described as two isosceles triangles (Zn1Zn2Fe1 and Zn1'Zn2'Fe1') which are linked through symmetry-related phenolate oxygen atoms (O7, O7') of two 3.2111 (Harris notation⁶¹) saphCOO²⁻ ligands, which bridge exclusively three Zn^{II} atoms (Zn1, Zn1', Zn2 and their symmetry equivalents). The Zn1O7Zn1'O7' rhombus is perfectly planar (due to symmetry); its sides are 1.988(6) and 2.071(5) Å, its angles are 79.7(2) and

Table 2 Selected interatomic distances (Å) and angles (°) for the {Zn₄Cr₂} complex, **2**·4MeCN·2EtOH^a

Interatomic distances			
Zn1···Cr1	4.545(2)	Zn1–O6	1.957(2)
Zn1···Cr1'	9.063(2)	Zn1–O13	1.977(2)
Zn1···Zn2	4.804(2)	Zn1–O9	1.960(2)
Zn1···Zn2'	6.633(2)	Zn2–O7	2.013(2)
Zn1···Zn1'	11.175(1)	Zn2–O3'	2.006(2)
Zn2···Cr1	4.478(2)	Zn2–N3	2.048(2)
Zn2···Cr1'	4.993(2)	Cr1–O4	1.940(2)
Zn2···Zn2'	3.044(1)	Cr1–O2	1.993(2)
Cr1···Cr1'	8.984(2)	Cr1–N2	2.066(2)
Bond angles			
O6–Zn1–O9	130.5(1)	O7–Zn2–O8	144.9(1)
O6–Zn1–O13	117.3(1)	O3'–Zn2–O7	117.5(1)
O6–Zn1–O10	102.5(1)	O3'–Zn2–N3	98.0(1)
O9–Zn1–O13	98.7(1)	O3'–Zn2–O7'	96.8(1)
O9–Zn1–O10	98.7(1)	O4–Cr1–O2	170.4(1)
O13–Zn1–O10	105.8(1)	O5–Cr1–N1	176.3(1)
N3–Zn2–O7'	165.2(1)	O1–Cr1–N2	171.9(1)

^a Symmetry operation used to generate equivalent atoms: (') $-x + 1, -y + 1, -z + 1$.

100.3(2)°, while the diagonal is 3.118(2) Å. The bridging of Fe1 and Zn2 is achieved by the syn, anti carboxylate group (O5, O6) of a 2.1111 saphCOO²⁻ ligand. Zn1 and Zn2 are connected through the syn, anti carboxylate group (O8, O9) of the above mentioned 3.2111 ligand. Zn1' and Fe1 are linked through the syn, anti carboxylate group (O2, O3) of a second 2.1111 saphCOO²⁻ ligand. There is no direct linking between Zn1 and Fe1 through monoatomic or triatomic bridges. The phenolate oxygen atoms of the 2.1111 ligands (O4, O1) are terminally ligated to Fe1. Thus, there are four 2.1111 and two 3.2111 saphCOO²⁻ groups in the whole molecule (Fig. 2). A terminal EtOH molecule (O13) and a highly anisobidentate chelating nitrate ion (O10, O11) complete 5-coordination at Zn2. Considering the latter,

Table 1 Selected interatomic distances (Å) and angles (°) for the {Zn₄Fe₂} complexes, **1**·4CH₂Cl₂·2EtOH and **3**·4CH₂Cl₂·2EtOH

1 ·4CH ₂ Cl ₂ ·2EtOH ^a				3 ·4CH ₂ Cl ₂ ·2EtOH ^b			
Interatomic distances				Interatomic distances			
Zn1···Zn1'	3.118(2)	Zn2–O9	1.924(6)	Zn1···Zn1'	3.095(2)	Zn2–O9	1.927(4)
Zn2···Zn2'	11.349(2)	Zn2–O6	1.946(6)	Zn2···Zn2'	11.336(2)	Zn2–O6	1.967(4)
Fe1···Fe1'	9.022(2)	Zn2–O13	2.025(6)	Fe1···Fe1'	9.111(2)	Zn2–O13	2.055(5)
Fe1···Zn1	4.505(2)	Zn2–O10	2.040(7)	Fe1···Zn1	4.468(2)	Zn2–O10	2.025(4)
Fe1···Zn2	4.547(2)	Zn2···O11	2.566(6)	Fe1···Zn2	4.470(2)	Zn2···O11	2.558(6)
Fe1···Zn2'	9.189(2)	Fe1–O1	1.900(6)	Fe1···Zn2'	9.262(3)	Fe1–O1	1.903(4)
Zn1···Zn2'	6.745(2)	Fe1–O5	1.992(6)	Zn1···Zn2'	6.732(2)	Fe1–O5	1.990(4)
Zn1–O7	1.988(6)	Fe1–N1	2.140(8)	Zn1–O7	1.998(4)	Fe1–N1	2.124(5)
Zn1–N3	2.070(7)	Fe1–N2	2.181(8)	Zn1–N3	2.072(5)	Fe1–N2	2.221(5)
Bond angles				Bond angles			
O7–Zn1–O3'	120.1(2)	O11···Zn2–O10	54.4(3)	O7–Zn1–O3'	114.7(2)	O11···Zn2–O10	54.5(3)
O7–Zn1–O7'	79.7(2)	O11···Zn2–O6	91.5(2)	O7–Zn1–O7'	81.1(2)	O11···Zn2–O6	91.0(3)
O7–Zn1–O8	140.9(2)	O11···Zn2–O13	143.2(3)	O7–Zn1–O8	142.3(2)	O11···Zn2–O13	146.1(3)
O7'–Zn1–N3	167.1(2)	Zn1–O7–Zn1'	100.3(2)	O7'–Zn1–N3	168.3(2)	Zn1–O7–Zn1'	98.1(2)
O13–Zn2–O10	89.2(3)	O4–Fe1–O2	158.1(2)	O13–Zn2–O10	92.1(2)	O4–Fe1–O2	155.7(2)
O9–Zn2–O10	111.1(3)	O5–Fe1–N1	172.0(3)	O9–Zn2–O10	113.7(2)	O5–Fe1–N1	168.4(2)
O9–Zn2–O13	102.1(3)	O1–Fe1–N2	168.3(3)	O9–Zn2–O13	103.0(2)	O1–Fe1–N2	166.2(2)
O11···Zn2–O9	88.4(3)	N1–Fe1–N2	103.1(3)	O11···Zn2–O9	87.5(3)	N1–Fe1–N2	105.3(2)

^a Symmetry operation used to generate equivalent atoms: (') $-x, -y - 1, -z - 1$. ^b Symmetry operation used to generate equivalent atoms: (') $-x + 1, -y + 1, -z + 2$.



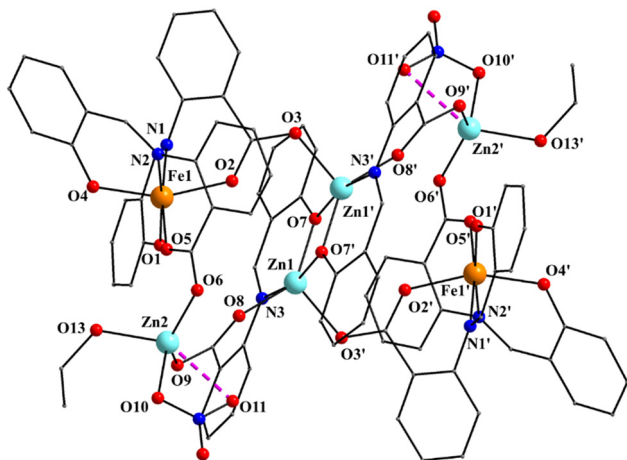


Fig. 1 Partially labeled plot of the molecule $[Zn_4Fe_2(saphCOO)_6(NO_3)_2(EtOH)_2]$ that is present in the crystal structure of **1**·4CH₂Cl₂·2EtOH. The dashed lines indicate a weakly bonding interaction. Symmetry operation used to generate equivalent atoms: ($'$) $-x, -y - 1, -z - 1$.

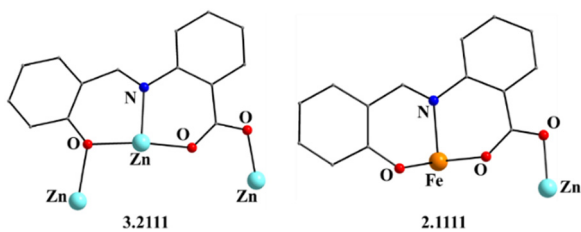


Fig. 2 The coordination modes (using Harris notation) of the $saphCOO^{2-}$ ligands in complex **1**·4CH₂Cl₂·2EtOH; four ligands adopt the 2.1111 ligation mode and two the 3.2111 one.

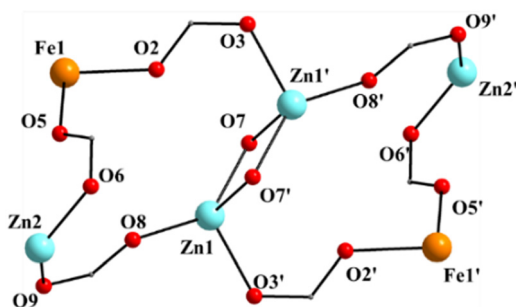


Fig. 3 The labeled core of **1**; the primes ($'$) are used for atoms generated by the symmetry operation $-x, -y - 1, -z - 1$.

the anisobidentate chelating character is indicated by the Zn2–O_{nitrate} bond lengths [2.040(7), 2.566(6) Å] which are significantly different; thus, the O11 could be considered as semicoordinated and its bond to Zn2 is drawn with a dashed line in Fig. 1. From Fig. 1 and the above discussion, it is clear that the coordination spheres are of the $\{Fe1O_4N_2\}$, $\{Zn1O_4N\}$ and $\{Zn2O_5\}$ types. Considering the triatomic carboxylate bridges as parts of the core, this is $\{Zn_4Fe_2(\mu-OR)_2(\eta^1:\eta^1:\mu-O_2CR')_4(\eta^1:\eta^1:\mu-O_2CR'')_2\}^{6+}$, where R, R' and R'' are parts of the $saphCOO^{2-}$ ligands.

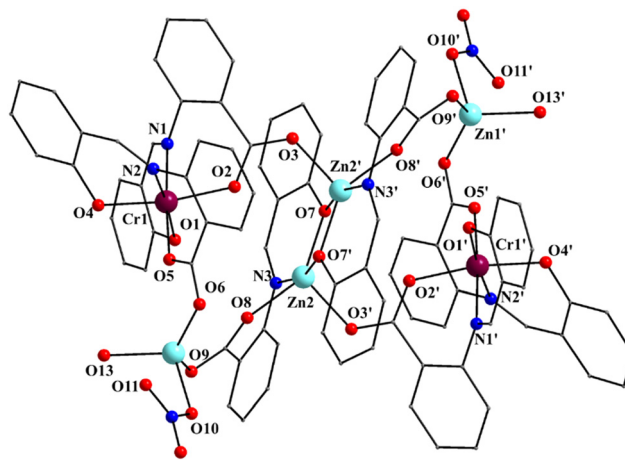


Fig. 4 Partially labeled plot of the molecule $[Zn_4Cr_2(saphCOO)_6(NO_3)_2(H_2O)_2]$ that is present in the crystal structure of **2**·4MeCN·2EtOH. The atom labeling scheme is similar to that adopted for **1** and **3**, the only difference being that the central Zn^{II} atoms of the planar rhombus are labeled as Zn2/Zn2' and the outer ones as Zn1/Zn1' in **2**, whereas the inverse applies for **1** and **3** (Fig. 1 and Fig. S1, ESI[†]). Symmetry operation used to generate equivalent atoms: ($'$) $-x + 1, -y + 1, -z + 1$.

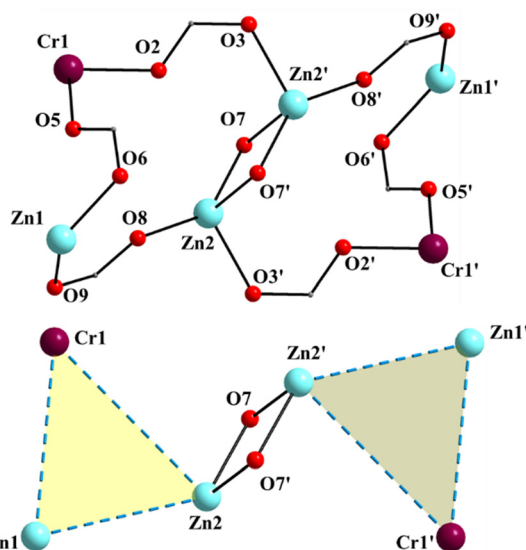


Fig. 5 The labeled core of **2** (up) and a view of the metal topology (also including the phenolate monoatomic bridging oxygen atoms) of the molecule (down). The primes are used for atoms generated by the symmetry operation $-x + 1, -y + 1, -z + 1$.

The Zn–O/N bond lengths are unremarkable,^{42,62} while the Fe^{III}–O/N bond distances are typical for high-spin iron(III) centers in an octahedral environment.^{42,43} The Fe^{III} coordination geometry is distorted octahedral, with the *trans* angles being in the range 158.1(2)–172.0(3)°. The Zn1 (and its symmetry equivalent) coordination geometry may be described as highly distorted square pyramidal, with the carboxylate atom O3' occupying the apical position. Analysis of the shape-determining angles using the approach of Anderson, Reedijk *et al.*⁶³ yields a value for the trigonality index, τ , of 0.45 for this



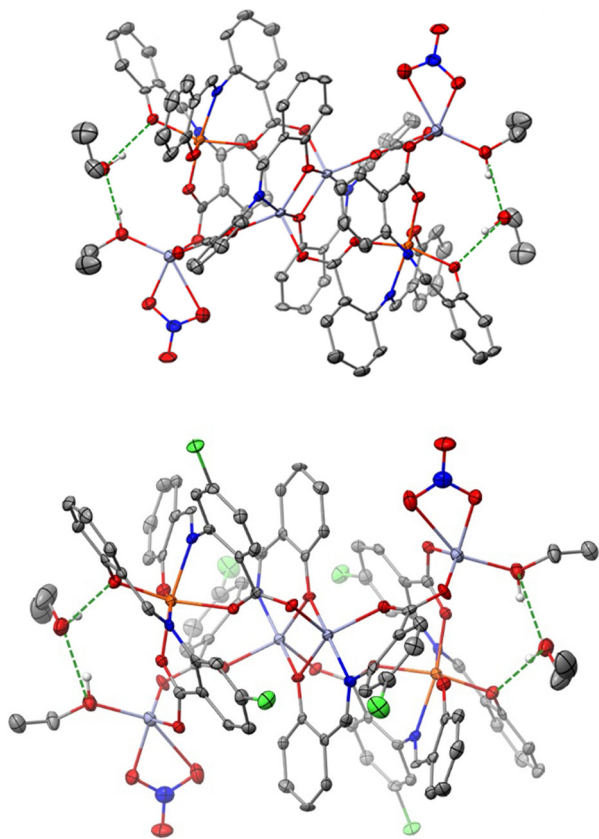


Fig. 6 ORTEP-type views of the complexes **1**·4CH₂Cl₂·2EtOH (top) and **3**·4CH₂Cl₂·2EtOH (bottom), and the two hydrogen bonded lattice EtOH molecules in the crystal at 120 K. Thermal ellipsoids are depicted at a 50% probability level. Lattice CH₂Cl₂ molecules and H atoms are omitted for clarity, except those involved in H-bonding. H bonds are illustrated with dashed green lines. C, grey; H, white; N, blue; O, red; Cl, light green; Fe, orange; Zn, light blue.

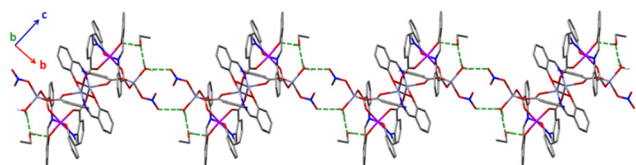


Fig. 7 Stick representation of the H-bonded molecules **2** forming an 1D H-bonded network. H atoms (except those involved in H bonds) and lattice MeCN molecules are omitted for clarity. H bonds are depicted in dashed green lines. C, grey; H, white; N, blue; O, red; Cr, purple; Zn, light blue.

metal ion ($\tau = 0$ and 1.0 for ideal square pyramidal and trigonal bipyramidal geometry, respectively). Although the τ value for Zn2 is significantly smaller (0.19) than that for Zn1, its geometry also appears highly distorted; it may be described as square pyramidal with the nitrate oxygen O10 at the apex of the pyramid. Reasons for the distortion are the small basal plane angles [143.2(3) and 131.3(3)°], significantly less than the ideal value of 180°, and the small bite angle of $\sim 55^\circ$ of the anisobidentate chelating NO₃⁻.

Complex **3**·4CH₂Cl₂·2EtOH is isostructural with **1**·4CH₂Cl₂·2EtOH, but not isomorphous (Table S1, ESI[†]). As it is obvious from Table 1 and Fig. 1, Fig. S1 (ESI[†]), the centrosymmetric molecules of **1** and **3** are very similar (for convenience, an analogous atom labeling scheme has been adopted). Again the 4ClSaphCOO²⁻ ligands adopt similar coordination modes (Fig. S2 and Fig. 2, ESI[†]). As in **1**, the nitrate groups are anisobidentate in **3**, the coordination spheres are of the {Fe1O₄N₂}, {Zn1O₄N} and {Zn2O₅} types, and the core is again {Zn₄Fe₂(μ -OR)₂(η^1 : η^1 : μ -O₂CR')₄(η^1 : η^1 : μ -O₂CR'')₂}⁶⁺. Thus, the Cl atom in the position 4 of the aminobenzoic aromatic ring has no influence on the molecular structure.

Complex **2**·4MeCN·2EtOH crystallizes in the triclinic space group *P* $\bar{1}$. Its structure consists of centrosymmetric hexanuclear [Zn₄Cr₂(saphCOO)₆(NO₃)₂(H₂O)₂], and lattice MeCN and EtOH molecules in an 1:4:2 ratio. The molecule of **2** has a rather similar structure to that of **1**, with the replacement of the Fe^{III} atoms in the latter by the Cr^{III} atoms in the former (Fig. 1–5 and Fig. S3, ESI[†]). There are two differences in the molecular structures of the two complexes. First, in **2** the outer Zn^{II} atoms (Zn1/Zn1' in Fig. 4) are bound to two aqua ligands (the corresponding terminal ligands are EtOH molecules in **1**). And second, the terminal nitrate ligands are clearly monodentate [the Zn1··O11/Zn1'··O11' distance is ~ 2.78 Å. *i.e.* non-bonding] in **2** as opposed to **1** in which these groups are anisobidentate; as a result the coordination geometry at Zn1 may be better described as distorted tetrahedral, the donor atom – Zn1/Zn1' – donor atom angles being in the 98.7(1)–130.5(1) range (Table 2). The Cr–N/O bond lengths are typical for octahedral Cr^{III} centers.^{44,46,64,65}

We now discuss the intermolecular interactions in the three structures. In **1**·4CH₂Cl₂·2EtOH and **3**·4CH₂Cl₂·2EtOH, each polynuclear molecule is H-bonded to lattice EtOH molecules, both as donor and as acceptor (Fig. 6 and Fig. S4, ESI[†]). The intermolecular distances are $d(\text{O}_{\text{lattice ethanol}} \cdots \text{O}_{\text{phenolate}}) = 2.730(3)$ Å and $d(\text{O}_{\text{lattice ethanol}} \cdots \text{O}_{\text{coordinated ethanol}}) = 2.687(4)$ Å in **1**·4CH₂Cl₂·2EtOH, and $d(\text{O}_{\text{lattice ethanol}} \cdots \text{O}_{\text{phenolate}}) = 2.719(3)$ Å and $d(\text{O}_{\text{coordinated ethanol}} \cdots \text{O}_{\text{lattice ethanol}}) = 2.698(3)$ Å in **3**·4CH₂Cl₂·2EtOH. Even though the two compounds are not isomorphous, the packing is similar with four dichloromethane molecules per hexanuclear complex filling the void space (Fig. S4 and S5, ESI[†]).

In **2**·4MeCN·2EtOH, each polynuclear molecule is H-bonded to two lattice EtOH molecules, both as donor and as acceptor (Fig. 7 and Fig. S6, ESI[†]), with intermolecular distances of $d(\text{O}_{\text{lattice ethanol}} \cdots \text{O}_{\text{phenolate}}) = 2.668(3)$ Å and $d(\text{O}_{\text{coordinated water}} \cdots \text{O}_{\text{lattice ethanol}}) = 2.644(3)$ Å. The coordinated H₂O molecule is also H-bonded to a “free” oxygen atom of the coordinated nitrate group of a neighboring hexanuclear molecule [$d(\text{O} \cdots \text{O}) = 2.775(3)$ Å], forming an 1D H-bonded network in the crystal (Fig. 7). Four lattice MeCN molecules per complex are also present and fill the void space. The shortest intermolecular metal··metal distances are 12.175 Å (**1**·4CH₂Cl₂·2EtOH), 7.733 Å (**3**·4CH₂Cl₂·2EtOH) and 7.629 Å (**2**·4MeCN·2EtOH).

Space-filling diagrams of **1** and **3** are shown in Fig. S7 and S8 (ESI[†]), respectively. The outer C··C distances in the molecules are *ca.* 1.9 nm.



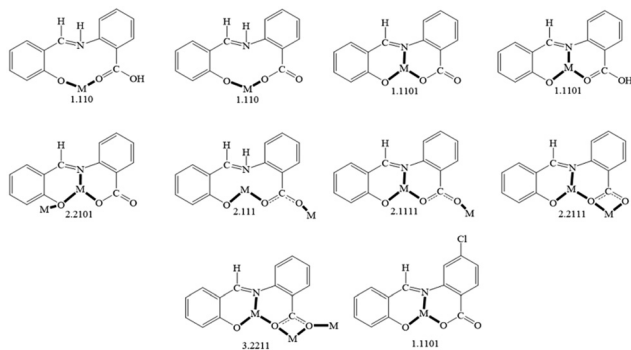


Fig. 8 The to-date crystallographically observed coordination modes of saphHCOOH, saphHCOO⁻, saphCOO²⁻ and 4ClsaphCOO²⁻, and the Harris notation that describes these modes; complexes containing the neutral or the singly deprotonated 4ClsaphHCOOH ligand have not yet been reported. The new ligation mode 3.2111 of the present work (Fig. 2 and Fig. S3, ESI[†]) is not included in the figure. Coordination bonds have been drawn with bold lines.

Complexes **1** and **3** join a rather small family of structurally characterized metal complexes containing the saphCOO²⁻ and saphHCOO⁻ ligands (selected compounds are described in ref. 29–33 and 66–69); most of them possess the doubly deprotonated ligand. As mentioned in “Introduction”, these are the first heterometallic complexes based on these ligands. On the contrary, **2** is only the second characterized complex with any form of 4ClsaphHCOOH as ligand, the first being [Cu(4ClsaphCOO)(phen)].^{36,37} For convenience, the to-date crystallographically established coordination modes of the two ligands are illustrated in Fig. 8.

The ligation mode 3.2111 (Fig. 2 and Fig. S3, ESI[†]) has not been observed before. The 2.1111 mode (Fig. 2 and 8) has been established only in few complexes of saphCOO²⁻,^{66–69} whereas this mode is new for 4ClsaphCOO²⁻.

Complexes **1**, **3** and **2** are members of families that have heterometallic Zn^{II}–Fe^{III} (selected literature is given in ref. 39–43, 62 and 64) and Zn^{II}–Cr^{III} (for example, see ref. 44–47, 64, 65 and 70) complexes, respectively. The nuclearity {Zn₄Fe₂^{III}} has been observed once,⁶² whereas the nuclearity {Zn₄Cr₂^{III}} was unknown prior to this work.

IR, Raman and UV/Vis spectra

The three complexes were characterized by vibrational and solution UV/Vis spectroscopies on well dried (*i.e.* as lattice solvent-free) samples (Fig. 9 and Fig. S9–S13, ESI[†]).

The IR and Raman spectra of the complexes are very similar in accordance with their similar structures. The weak-to-medium intensity broad IR band at 3482–3420 cm⁻¹ is assigned to the $\nu(\text{OH})$ vibration of the coordinated EtOH (**1**, **3**) and H₂O (**2**) molecules; the broadness of the band suggests H bonding.⁵¹ As expected, this mode is hardly seen in the Raman spectra. The IR spectra exhibit a strong band at ~1595 cm⁻¹ which is assigned to the $\nu(\text{C}=\text{N})$ vibration of the Schiff-base linkage,^{51,52} most probably overlapping with an aromatic stretch. This spectral mode appears as a strong peak at ~1615 cm⁻¹ in **1** and **3**, and as a medium-intensity peak at 1630 cm⁻¹ (**2**) in the

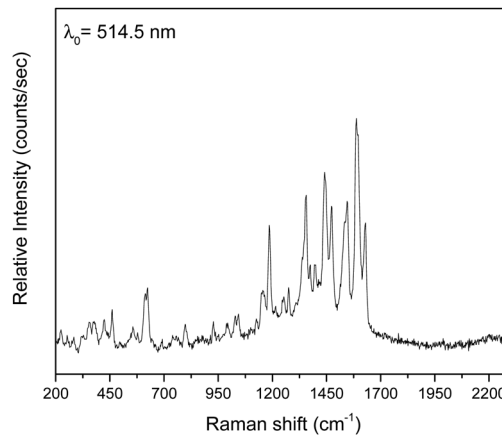


Fig. 9 The Raman spectrum of a dried sample of **2** in the 2300–200 cm⁻¹ region.

Raman spectra.⁷¹ The IR spectra exhibit a medium to strong band at *ca.* 1385 cm⁻¹, characteristic of the $\nu_3(E')[\nu_d(\text{NO})]$ mode of the planar D_{3h} ionic NO₃⁻;⁷² however, such nitrates are not present in the crystal structure of the complexes. The appearance of this band indicates that the nitrate ligands (or an amount of them) in the samples are replaced by bromides that are present in the KBr matrix (used for the preparation of pellets), and so ionic nitrates (KNO₃) are produced;⁷³ it is well known that this replacement is facilitated by the pressure applied. In accordance with this explanation, the peak at ~1385 cm⁻¹ is always absent in the Raman spectra of the complexes. In these spectra, the peaks at 1458–1442 and 1317–1308 cm⁻¹ are assigned to the $\nu_5(B_2)[\nu_{\text{as}}(\text{NO}_2)]$ and $\nu_1(A_1)[\nu_s(\text{NO}_2)]$ modes, respectively, of the nitrate group assuming C_{2v} symmetry; their separation is small (~150 cm⁻¹) indicating monodentate nitrates.⁷² Thus, from the Raman spectroscopy viewpoint the nitrate ligands appear monodentate, suggesting that the anisobidentate chelating character in **1** and **3** is not reflected in the spectra. A larger separation (~200 cm⁻¹) of the two highest wavenumber stretching nitrogen–oxygen is expected for “normal” bidentate chelating nitrate ligands.⁷² The fact that the ~1450 and ~1300 cm⁻¹ bands are present in the IR spectra is an indication that there is an amount of coordinated nitrate group still present in the samples and only a percentage of the whole NO₃⁻ content has been transformed to ionic nitrates. The location of the carboxylate stretching bands in the expected 1600–1300 cm⁻¹ region⁷² is difficult due to the appearance of aromatic and nitrate stretching vibrations in this region. The IR bands at 1550–1540 and *ca.* 1380 cm⁻¹ are tentatively assigned^{72,74} to the $\nu_{\text{as}}(\text{CO}_2)$ and $\nu_s(\text{CO}_2)$ vibrations respectively, the latter overlapping with the ionic nitrate stretching vibration $\nu_3(E')[\textit{vide supra}]$. Only in the spectrum of **3** (Fig. S11, ESI[†]), the $\nu_s(\text{CO}_2)$ band (at 1401 cm⁻¹) is well separated from the nitrate band. The large $\nu_{\text{as}}(\text{CO}_2)$ – $\nu_s(\text{CO}_2)$ difference (~160 cm⁻¹) is indicative of the bidentate bridging ligation of the carboxylate groups of saphCOO²⁻ and 4ClsaphCOO²⁻.^{72,74} The $\nu_{\text{as}}(\text{CO}_2)$ and $\nu_s(\text{CO}_2)$ Raman peaks appear at *ca.* 1540 and *ca.* 1275 cm⁻¹, respectively,



with the latter not seen clearly in the spectrum of **3**; again the large separation suggests bidentate bridging behavior.⁷²

The UV/Vis spectra of **1–3** were recorded in CH₂Cl₂ (Fig. S13, ESI†). The molar conductivities, Λ_M , are negligible (1–4 S cm² mol⁻¹), suggesting the absence of ionic species in solution.⁷⁵ This fact, in combination with the non-donor properties of CH₂Cl₂, might indicate that the molecular structures of the complexes are retained in solution. In the spectra of **1** and **3**, the bands below 300 nm are due to transitions of the aromatic ring, the longest wavelength maximum also having a –CH=N– transition character.⁷⁶ The 380, 405 and 510 nm bands are assigned to ligand-to-metal charge transfer (LMCT) transitions,⁷⁷ *i.e.* from ligands' π orbitals to the t_{2g} orbitals of iron(III). Because of the oxidizing power of Fe^{III}, LMCT bands often obscure the very low intensity d–d transitions. The weak band at *ca.* 585 nm may be due to the ${}^6A_{1g} \rightarrow {}^4T_{2g}$ transition⁷⁷ in a high-spin 3d⁵ octahedral system. The interpretation of the electronic spectrum of **2** is not easy. The bands at 225 and 240 nm are assigned⁷⁷ to transition within the π system of the aromatic rings, the longest wavelength maximum possibly also having a –CH=N– transition character.⁷⁶ Since Cr(III) is neither a good reducing nor a good oxidizing agent, charge transfer bands tend not to obscure the three spin-allowed transitions. The bands at 280, 420 and 522 nm are attributed⁷⁷ to the ${}^4A_{2g} \rightarrow {}^4T_{1g}$ (P), ${}^4A_{2g} \rightarrow {}^4T_{1g}$ (F) and ${}^4A_{2g} \rightarrow {}^4T_{2g}$ d–d transitions, respectively, in an octahedral 3d³ crystal field. The possibility the 280 nm band to have a mixed –CH=N/d–d character can not be ruled out. The band at 325 nm can be tentatively assigned to a LMCT transition, while that at 583 nm to the spin-forbidden ${}^4A_{2g} \rightarrow {}^2T_{2g}$, 2E_g transition.⁷⁷ The longest wavelength spin-allowed d–d transition at 522 nm gives directly the e_g – t_{2g} gap (10 Dq) which is $\sim 19\,150$ cm⁻¹, typical for octahedral Cr^{III} complexes in a mixed N/O environment.⁷⁷

⁵⁷Fe Mössbauer spectra

Zero-field Mössbauer spectra of powdered samples of well dried **1** and **3** were recorded at 300 and 80 K. Spectra are presented in Fig. 10 and Fig. S14 (ESI†). At 300 K, the spectrum of **1** consists of a relative broad doublet with an apparent isomer shift value (δ) of ~ 0.35 mm s⁻¹ with an estimated quadruple splitting parameter, ΔE_Q , of ~ 0.6 mm s⁻¹. The δ value is consistent with a high-spin Fe^{III} ion in an octahedral environment comprising N/O-donors.⁷⁸ A more accurate determination of ΔE_Q is hindered by the broadness of the peak. The broadness of the spectrum is attributed to relaxation effects and this is often observed in isolated high-spin ferric ions in the solid state.⁷⁹ In comparison to **3**, the 300 K spectrum of **1** exhibits already a broad background. At 80 K, the doublet becomes broader and the broad background increases. We attribute this behavior to spin relaxation effects.

The Mössbauer behavior of **3** is similar to that of **1**. At room temperature, the spectrum consists of a broad absorption peak corresponding to a δ value of 0.38 mm s⁻¹. Again this value is consistent with a high-spin Fe^{III} ion possessing a mixed O/N-donor coordination sphere.⁷⁸ The ΔE_Q value is estimated to be ~ 0.5 mm s⁻¹. At 80 K, the central peak becomes broader. At the same time, a broad background develops having the behavior

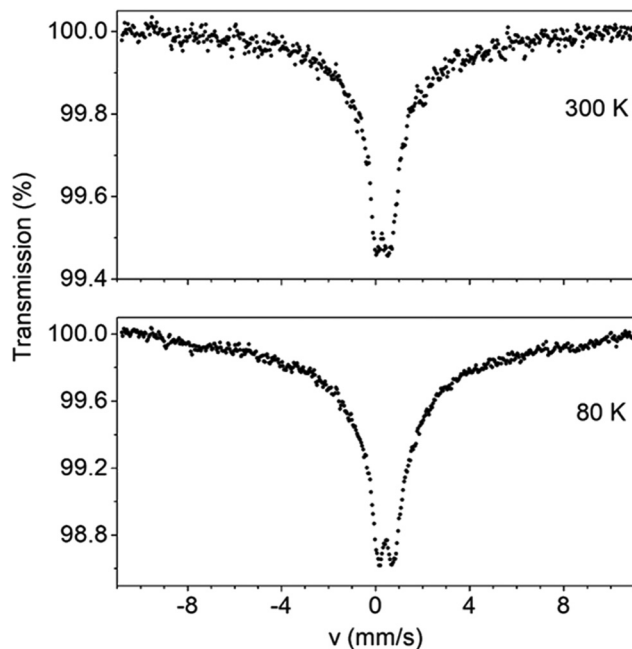


Fig. 10 Mössbauer spectra of powdered samples of dried complex **1** recorded at 300 and 80 K in zero applied field.

of an unresolved magnetic sextet. This is consistent (like the broadness of the spectrum of **1**⁷⁹) with magnetic relaxation effects. As the temperature decreases, the spin–lattice relaxation rate decreases leading to the conversion of the Mössbauer spectrum from a doublet to sextet.

Magnetic properties in brief

Variable-temperature (1.8–300 K) dc magnetic susceptibility studies were performed on powdered microcrystalline complexes of the three complexes at 0.1 T. Data are shown in Fig. 11, 12 and Fig. S15–S18 (ESI†). The crystals were filtered directly from mother liquor and immediately prepared for measurements. The χT value of 1·4CH₂Cl₂·2EtOH at room temperature is 9.8 cm³ K mol⁻¹, identical with the expected value ($g = 2.12$) for two non-interacting high-spin Fe^{III} centers (χ is the molar magnetic susceptibility). The value of the χT product remains practically constant in the 300–20 K range and then decreases reaching a value of 8.9 cm³ K mol⁻¹ at 1.85 K. This behavior is indicative of a very weak (if any) antiferromagnetic exchange interaction between the paramagnetic metal spins. The data have been subjected to a least-squares fit to the expression⁸⁰ derived from the spin-Hamiltonian $\hat{H} = -2J(\hat{S}_1 \cdot \hat{S}_2)$, with $S_1 = S_2 = 5/2$. The calculated value is $J/k_B = -0.03(1)$ K (with $g = 2.12(5)$). Magnetization data at 1.85 K are approaching saturation at 7 T with a value of 11.0 μ_B for two independent $S = 5/2$ ions and a g value of 2.10(5). Data for complex 3·4CH₂Cl₂·2EtOH are similar with a room-temperature χT value of 9.1 cm³ K mol⁻¹ ($g = 2.04(5)$) and $J/k_B = -0.06(1)$ K.

The χT value of 2·4MeCN·2EtOH at room temperature is 4.0 cm³ K mol⁻¹, close to the expected value ($g = 2.06$) for two non-interacting $S = 3/2$ Cr^{III} centers. The value of the χT product remains constant in the 300–15 K range and then decreases



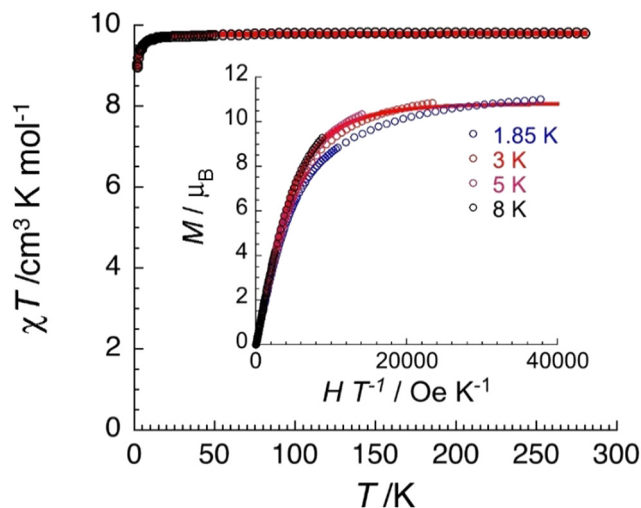


Fig. 11 Temperature dependence of the χT product (where χ is the molar magnetic susceptibility that equals M/H per complex, and T the temperature) collected in an applied dc magnetic field (H) of 0.1 T for $1.4\text{CH}_2\text{Cl}_2 \cdot 2\text{EtOH}$. The solid red line is the best fit of the experimental data to an Heisenberg $S_{\text{Fe}} = 5/2$ spin dimer model as discussed in the text. Inset: Field dependence of the magnetization (M) for $1.4\text{CH}_2\text{Cl}_2 \cdot 2\text{EtOH}$ below 8 K plotted as M vs. H/T . The solid red line is the best fit of the experimental data to two $S = 5/2$ Brillouin functions as discussed in the text.

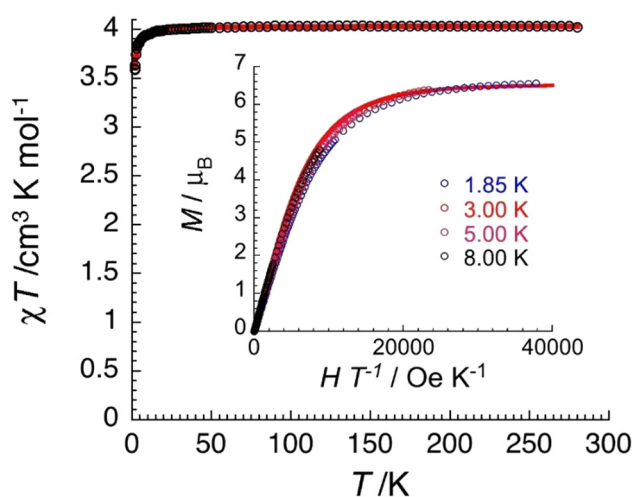


Fig. 12 Temperature dependence of the χT product (where χ is the molar magnetic susceptibility that equals M/H per complex, and T the temperature) collected in an applied dc magnetic field (H) of 0.1 T for $2.4\text{MeCN} \cdot 2\text{EtOH}$. The solid red line is the best fit of the experimental data to an Heisenberg $S_{\text{Cr}} = 3/2$ spin dimer model as discussed in the text. Inset: field dependence of the magnetization (M) for $2.4\text{MeCN} \cdot 2\text{EtOH}$ below 8 K plotted as M vs. H/T . The solid red line is the best fit of the experimental data to two $S = 3/2$ Brillouin functions as discussed in the text.

reaching a value of $3.6 \text{ cm}^3 \text{ K mol}^{-1}$ at 1.85 K. This behavior suggests a very weak antiferromagnetic exchange interaction between the Cr^{III} spins. The data were fitted to the expression derived from the HDVV spin-Hamiltonian $\hat{H} = -2J(\hat{S}_1 \cdot \hat{S}_2)$ giving a J/k_{B} value of $-0.16(1) \text{ K}$ (with $g = 2.07(5)$). Magnetization data have reached saturation at 7 T with a value of $6.6\mu_{\text{B}}$ for two independent $S = 3/2$ ions with $g = 2.20(5)$.

The negligible magnetic coupling for the complexes was expected considering the long ($>7.5 \text{ \AA}$, *vide supra*) intra- and intermolecular distances between the paramagnetic metal ions. However, cases have been reported⁴⁴ in $\{\text{Zn}^{\text{II}}\text{Cr}_2^{\text{III}}\}$ complexes, where appreciable spin coupling between terminal Cr^{III} ions separated by *ca.* 7 \AA , is operated.

Conclusions and perspectives

The chemical message of this work is the ability of saphHCOOH and 4Cl saphHCOOH to form heterometallic 3d–3d' complexes. Complexes 1–3 are the first heterometallic species based on these ligands. Their donor-atom system is ideal for both tridentate chelating $\text{O}_{\text{phenolate}}$, N_{imine} , $\text{O}_{\text{carboxylate}}$ and bridging behavior; candidate bridging atoms are the “free” (*i.e.* not coordinated) carboxylate oxygen, and both the coordinated phenolate and carboxylate atoms. *A priori* prediction for the preference for heterometallic or homometallic species is not possible. More judicious choice of the different metal ions is necessary to enforce the formation of heterometallic complexes. From the inorganic chemistry viewpoint, the complexes have interesting molecular structures, metal topologies, and enrich the groups of $\text{Zn}^{\text{II}}\text{Fe}^{\text{III}}$ and $\text{Zn}^{\text{II}}\text{Cr}^{\text{III}}$ compounds; moreover, the $\{\text{Zn}_4\text{Cr}_2^{\text{III}}\}$ nuclearity is new, the $\{\text{Zn}_4\text{Fe}_2^{\text{III}}\}$ one has been characterized for the second time and the 3.2111 coordination mode of $\text{saphCOO}^{2-}/4\text{Cl saphCOO}^{2-}$ is observed for the first time. Given the long distance between the paramagnetic Fe^{III} and Cr^{III} ions, the magnetic exchange interactions are extremely weak and of antiferromagnetic nature.

With knowledge and experience obtained in the present study, our efforts are directed, among others, to: (1) the preparation of heterometallic 3d–3d' and 3d–4f complexes of the singly deprotonated (saphHCOO^- , 4Cl saphHCOO^-) ligands; (2) the replacement of Zn^{II} with the other metal ions of Group 12 (Cd^{II} , Hg^{II}) to see if this change affects the chemical and structural identity of the products; (3) the use of two different paramagnetic metal ions, *e.g.* the pairs $\text{Ni}^{\text{II}}\text{Fe}^{\text{III}}$, $\text{Ni}^{\text{II}}\text{Cr}^{\text{III}}$, $\text{Cu}^{\text{II}}\text{Fe}^{\text{III}}$, $\text{Cu}^{\text{II}}\text{Cr}^{\text{III}}$, $\text{Cu}^{\text{II}}\text{Ln}^{\text{III}}$, $\text{Ni}^{\text{II}}\text{Ln}^{\text{III}}$ (Ln = trivalent lanthanoid), to bring them at short distances with the goal to obtain new polynuclear complexes with interesting magnetic properties; (4) the replacement of Fe^{III} in 1 and 3 with diamagnetic trivalent metals (*e.g.* Ga^{III} and In^{III}) or Ln^{III} ions aiming at the isolation of new species with photoluminescence properties based on the organic ligands or the 4f element, respectively; and (5) the incorporation of electron-releasing or electron-withdrawing (except Cl used in this work) non-donor substituents on one or both the aromatic rings, and study of their heterometallic coordination chemistry to investigate the effect of substituent(s) on the electronic and structural characteristics of the products.

Author contributions

Konstantinos N. Pantelis: data curation, formal analysis, investigation, methodology. Sotiris G. Skiadas: data curation, formal



analysis, investigation. Zoi G. Lada: data curation, formal analysis, investigation. Rodolphe Clérac: data curation, formal analysis, methodology, software, editing – original draft. Yiannis Sanakis: data curation, formal analysis, methodology, software, writing – original draft. Pierre Dechambenoit: conceptualization, investigation, methodology, software, writing – original draft. Spyros P. Perlepes: conceptualization, supervision, writing – original draft, writing – review and editing.

Conflicts of interest

There are no conflicts to declare.

Acknowledgements

We thank the Head of the Laboratory of Applied Molecular Spectroscopy, Research Director George A. Voyiatzis (ICE-HT/FORTH), for the access to the Raman facilities. R. C. and P. D. thank the University of Bordeaux, the Région Nouvelle Aquitaine, Quantum Matter Bordeaux (QMBx), the Centre National de la Recherche Scientifique (CNRS), and the Association Française de Magnétisme Moléculaire.

References

- M. G. Kanatzidis, R. Pöttgen and W. Jeitschko, *Angew. Chem., Int. Ed.*, 2005, **44**, 6996–7023.
- S.-W. Cheong and M. Mostovoy, *Nat. Mater.*, 2007, **6**, 13–20.
- N. Liu, C. Homann, S. Morfin, M. S. Kesanakurti, N. D. Calvert, A. J. Shuhendler, T. Al and E. Hemmer, *Nanoscale*, 2023, **15**, 19546–19556.
- J. S. Kanady, E. Y. Tsui, M. W. Day and T. Agapie, *Science*, 2011, **333**, 733–736.
- S. Mukherjee, J. A. Stull, J. Yano, T. C. Stamatatos, K. Pringouri, T. A. Stich, K. A. Abboud, R. D. Britt, V. K. Yachandra and G. Christou, *Proc. Natl. Acad. Sci. U. S. A.*, 2012, **109**, 2257–2262.
- R. Bagai and G. Christou, *Chem. Soc. Rev.*, 2009, **38**, 1011–1026.
- H. Miyasaka, M. Julve, M. Yamashita and R. Clérac, *Inorg. Chem.*, 2009, **48**, 3420–3437.
- J. D. Blakemore, R. H. Crabtree and G. W. Brudvig, *Chem. Rev.*, 2015, **115**, 12974–13005.
- J. L. Atwood and J. M. Lehn, *Comprehensive Supramolecular Chemistry*, Pergamon, Oxford, UK, 1996.
- M. O’Keeffe and O. M. Yaghi, *Chem. Rev.*, 2012, **112**, 675–702.
- D. Aguilà, L. A. Barrios, V. Velasco, O. Roubeau, A. Repollés, P. J. Alonso, J. Sesé, S. J. Teat, F. Luis and G. Aromí, *J. Am. Chem. Soc.*, 2014, **136**, 14215–14222.
- N. C. Anastasiadis, C. D. Polyzou, G. E. Kostakis, V. Bekiari, Y. Lan, S. P. Perlepes, K. F. Konidaris and A. K. Powell, *Dalton Trans.*, 2015, **44**, 19791–19795.
- D. Aguilà, Y. Prado, E. S. Koumoussi, C. Mathonière and R. Clérac, *Chem. Soc. Rev.*, 2016, **45**, 203–224.
- T. Iwazumi, A. Kusumoto, R. Takeshita, D. Kobayashi, H. Tokoro, K. Nakagawa and S.-I. Ohkoshi, *J. Electron Spectrosc. Relat. Phenom.*, 2024, **271**, 147421.
- A recent review from our group: Z. G. Lada, C. D. Polyzou, V. Nika, T. C. Stamatatos, K. F. Konidaris and S. P. Perlepes, *Inorg. Chim. Acta*, 2022, **539**, 120954.
- K. Liu, W. Shi and P. Cheng, *Coord. Chem. Rev.*, 2015, **289–290**, 74–122.
- L. Rosado Piquer and E. C. Sañudo, *Dalton Trans.*, 2015, **44**, 8771–8780.
- J. W. Sharples and D. Collison, *Coord. Chem. Rev.*, 2014, **260**, 1–20.
- H.-S. Wang, K. Zhang, Y. Song and Z.-Q. Pan, *Inorg. Chim. Acta*, 2021, **521**, 120318.
- A. Dey, J. Acharya and V. Chandrasekhar, *Chem. – Asian J.*, 2019, **14**, 4433–4453.
- C. D. Polyzou, C. G. Efthymiou, A. Escuer, L. Cunha-Silva, C. Papatrifiantafyllopoulou and S. P. Perlepes, *Pure Appl. Chem.*, 2013, **85**, 315–327.
- Z. G. Lada, E. Katsoulakou and S. P. Perlepes, in *Single-Molecule Magnets*, ed. M. Holyńska, Wiley-VCH, Weinheim, Germany, 2019, pp. 282–286.
- For a review from our group, see: S. T. Tsantis, D. I. Tzimopoulos, M. Holyńska and S. P. Perlepes, *Int. J. Mol. Sci.*, 2020, **21**, 555.
- L. Rigamonti, A. Forni, S. Righetto and A. Pasini, *Dalton Trans.*, 2019, **48**, 11217–11234.
- J. Long, *Front. Chem.*, 2019, **7**, 63.
- R. Molina-Hernández and A. Mederos, in *Comprehensive Coordination Chemistry II*, ed. J. A. McCleverty and T. J. Meyer, Elsevier, Amsterdam, The Netherlands, 2004, pp. 411–446.
- M. E. Belowich and J. F. Stoddart, *Chem. Soc. Rev.*, 2012, **41**, 2003–2024.
- C. D. Meyer, C. S. Joiner and J. F. Stoddart, *Chem. Soc. Rev.*, 2007, **36**, 1705–1723.
- I. C. Lazzarini, A. V. Funes, L. Carrella, L. Sorace, E. Rentschler and P. Alborés, *Eur. J. Inorg. Chem.*, 2014, 2561–2568.
- N. C. Anastasiadis, N. Lalioti, A. Terzis, V. Psycharis, C. P. Raptopoulou and S. P. Perlepes, *Inorg. Chem. Commun.*, 2015, **51**, 118–121.
- H. Ke, G.-F. Xu, Y.-N. Guo, P. Gamez, C. M. Beavers, S. J. Teat and J. Tang, *Chem. Commun.*, 2010, **46**, 6057–6059.
- I. C. Lazzarini, L. Carrella, E. Rentschler and P. Alborés, *Inorg. Chim. Acta*, 2016, **453**, 692–696.
- N. C. Anastasiadis, C. M. Granadeiro, J. Mayans, C. P. Raptopoulou, V. Bekiari, L. Cunha-Silva, V. Psycharis, A. Escuer, S. S. Balula, K. F. Konidaris and S. P. Perlepes, *Inorg. Chem.*, 2019, **58**, 9581–9585.
- E. C. Mazarakioti, J. Regier, L. Cunha-Silva, W. Wernsdorfer, M. Pilkington, J. Tang and T. C. Stamatatos, *Inorg. Chem.*, 2017, **56**, 3568–3578.
- A. A. Athanasopoulou, M. Pilkington, C. P. Raptopoulou, A. Escuer and T. C. Stamatatos, *Chem. Commun.*, 2014, **50**, 14942–14945.
- X. Li, C.-F. Bi, Y.-H. Fan, X. Zhang, X.-D. Wei and X.-M. Meng, *Transition Met. Chem.*, 2014, **39**, 577–584.



- 37 X. Li, D. Zhang, Z. Liu, Y. Xu and D. Wang, *Inorg. Chim. Acta*, 2018, **471**, 280–289.
- 38 A. G. J. Ligtenbarg, R. Hage, A. Meetsma and B. L. Feringa, *J. Chem. Soc., Perkin Trans. 2*, 1999, 807–812.
- 39 H. Machinaga, K. Matsufuji, M. Ohba, M. Kodera and H. Okawa, *Chem. Lett.*, 2002, 716–717.
- 40 P. Biswas, M. Ghosh, S. K. Dutta, U. Flörke and K. Nag, *Inorg. Chem.*, 2006, **45**, 4830–4844.
- 41 P. F. Teh, Y. Sharma, S. S. Pramana and M. Srinivasan, *J. Mater. Chem.*, 2011, **21**, 14999–15008.
- 42 A. Hazra, S. Bonakala, S. K. Reddy, S. Balasubramanian and T. K. Maji, *Inorg. Chem.*, 2013, **52**, 11385–11397.
- 43 J. L. Wong, R. F. Higgins, I. Bhowmick, D. X. Cao, G. Szigethy, J. W. Ziller, M. P. Shores and A. F. Heyduk, *Chem. Sci.*, 2016, **7**, 1594–1599.
- 44 D. Burdinski, E. Bill, F. Birkelbach, K. Wiegardt and P. Chaudhuri, *Inorg. Chem.*, 2001, **40**, 1160–1166.
- 45 A. Schoedel, A. J. Cairns, Y. Belmabkhout, L. Wojtas, M. Mohamed, Z. Zhang, D. M. Proserpio, M. Eddaoudi and M. J. Zaworotko, *Angew. Chem., Int. Ed.*, 2013, **52**, 2902–2905.
- 46 H. W. L. Fraser, G. S. Nichol, D. Uhrin, U. G. Nielsen, M. Evangelisti, J. Schnack and E. K. Brechin, *Dalton Trans.*, 2018, **47**, 11834–11842.
- 47 R. Alotaibi, E. Little, J. M. Fowler, A. Brookfield, R. W. Adams, A. Achari, G. A. Timco, G. F. S. Whitehead, N. F. Chilton, R. R. Nair, D. Collison and R. E. P. Winpenny, *Inorg. Chem.*, 2021, **60**, 15675–15685.
- 48 F. Troiani, A. Ghirri, M. Affronte, S. Carretta, P. Santini, G. Amoretti, S. Piligkos, G. Timco and R. E. P. Winpenny, *Phys. Rev. Lett.*, 2005, **94**, 207208.
- 49 M. Affronte, A. Ghirri, S. Carretta, G. Amoretti, S. Piligkos, G. A. Timco and R. E. P. Winpenny, *Appl. Phys. Lett.*, 2004, **84**, 3468–3470.
- 50 F. Moro, D. Kaminski, F. Tuna, G. F. S. Whitehead, G. A. Timco, D. Collison, R. E. P. Winpenny, A. Ardavan and E. J. L. McInnes, *Chem. Commun.*, 2014, **50**, 91–93.
- 51 S. T. Tsantis, V. Bekiari, C. P. Raptopoulou, D. I. Tzimopoulos, V. Psycharis and S. P. Perlepes, *Polyhedron*, 2018, **152**, 172–178.
- 52 N. C. Anastasiadis, D. A. Kalofolias, A. Philippidis, S. Tzani, C. P. Raptopoulou, V. Psycharis, C. J. Milios, A. Escuer and S. P. Perlepes, *Dalton Trans.*, 2015, **44**, 10200–10209.
- 53 K. I. Alexopoulou, A. Terzis, C. P. Raptopoulou, V. Psycharis, A. Escuer and S. P. Perlepes, *Inorg. Chem.*, 2015, **54**, 5615–5617.
- 54 D. Maniaki, I. Mylonas-Margaritis, J. Mayans, A. Savvidou, C. P. Raptopoulou, V. Bekiari, V. Psycharis, A. Escuer and S. P. Perlepes, *Dalton Trans.*, 2018, **47**, 11859–11872.
- 55 I. Mylonas-Margaritis, Z. G. Lada, A. A. Kitos, D. Maniaki, K. Skordi, A. J. Tasiopoulos, V. Bekiari, A. Escuer, J. Mayans, V. Nastopoulos, E. G. Bakalbassis, D. Papaioannou and S. P. Perlepes, *Dalton Trans.*, 2023, **52**, 8332–8343.
- 56 A. D. Westland and M. T. H. Tarafder, *Inorg. Chem.*, 1981, **20**, 3992–3995.
- 57 Z. H. Abd El-Wahab, *Spectrochim. Acta, Part A*, 2007, **67**, 25–38.
- 58 G. M. Sheldrick, *SADABS, ver. 2.03*, Bruker Analytical X-Ray Systems, Madison, WI, USA, 2000.
- 59 G. Sheldrick, *Acta Crystallogr., Sect. A: Cryst. Phys., Diffraction, Theor. Gen. Crystallogr.*, 2015, **71**, 3–8.
- 60 G. Sheldrick, *Acta Crystallogr., Sect. C: Cryst. Struct. Commun.*, 2015, **71**, 3–8.
- 61 R. A. Coxall, S. G. Harris, D. K. Henderson, S. Parsons, P. A. Tasker and R. E. P. Winpenny, *J. Chem. Soc., Dalton Trans.*, 2000, 2349–2356.
- 62 I. A. Lutsenko, M. A. Kiskin, N. N. Efimov, E. A. Ugolkova, Y. V. Maksimov, V. K. Imshennik, A. S. Goloveshkin, A. V. Khoroshilov, A. S. Lytvynenko, A. A. Sidorov and I. L. Eremenko, *Polyhedron*, 2017, **137**, 165–175.
- 63 A. W. Addison, T. N. Rao, J. Reedijk, J. van Rijn and G. C. Verschoor, *J. Chem. Soc., Dalton Trans.*, 1984, 1349–1356.
- 64 S. Sanz, H. M. O'Connor, V. Marti-Centelles, P. Comar, M. B. Pitak, S. J. Coles, G. Lorusso, E. Palacios, M. Evangelisti, A. Baldansuren, N. F. Chilton, H. Weihe, E. J. L. McInnes, P. J. Lusby, S. Piligkos and E. K. Brechin, *Chem. Sci.*, 2017, **8**, 5526–5535.
- 65 V. V. Semenaka, O. V. Nesterova, V. N. Kokozay, V. V. Dyakononko, R. I. Zubatyuk, O. V. Shishkin, R. Boča, J. Jezierska and A. Ozarowski, *Inorg. Chem.*, 2010, **49**, 5460–5471.
- 66 W.-Z. Ju, L. Shi, K. Chen and J.-Y. Xue, *Acta Crystallogr., Sect. C: Struct. Chem.*, 2005, **61**, m1427–m1428.
- 67 J. Wang, F. L. Bei, X. J. Yang, L. D. Lu and X. Wang, *J. Mol. Struct.*, 2002, **643**, 129–133.
- 68 S. S. Tonde, A. S. Kumbhar, S. B. Padhye and R. J. Butcher, *J. Inorg. Biochem.*, 2006, **100**, 51–57.
- 69 R. H. Laye and E. C. Sañudo, *Inorg. Chim. Acta*, 2009, **362**, 2205–2212.
- 70 F. K. Larsen, J. Overgaard, S. Parsons, E. Rentschler, A. A. Smith, G. A. Timco and R. E. P. Winpenny, *Angew. Chem., Int. Ed.*, 2003, **42**, 5978–5981.
- 71 F. R. Dollish, W. G. Fateley and F. F. Bentley, *Characteristic Raman Frequencies of Organic Compounds*, Wiley, New York, USA, 1974, pp. 110, 134–137.
- 72 K. Nakamoto, *Infrared and Raman Spectra of Inorganic and Coordination Compounds*, Wiley, New York, USA, 4th edn, 1986, pp. 121–124, 231–233, 254–257.
- 73 G. J. Kleywegt, W. G. R. Wiesmeijer, G. J. Van Driel, W. L. Driessen, J. Reedijk and J. H. Noordik, *J. Chem. Soc., Dalton Trans.*, 1985, 2177–2184.
- 74 G. B. Deacon and R. J. Phillips, *Coord. Chem. Rev.*, 1980, **33**, 227–250.
- 75 W. J. Geary, *Coord. Chem. Rev.*, 1971, **7**, 81–122.
- 76 C. N. R. Rao, *Ultra-Violet and Visible Spectroscopy*, Butterworths, London, UK, 1967, 2nd edn, pp. 20–33, 58–73.
- 77 A. B. P. Lever, *Inorganic Electronic Spectroscopy*, Elsevier, Amsterdam, The Netherlands, 2nd edn, 1984, pp. 329–332, 417–420, 450, 452, 453.
- 78 M. Savva, D. I. Alexandropoulos, M. Pissas, S. P. Perlepes, C. Papatriantafyllopoulou, Y. Sanakis and A. J. Tasiopoulos, *Dalton Trans.*, 2023, **52**, 6997–7008.
- 79 N. N. Greenwood and T. C. Gibbs, *Mössbauer Spectroscopy*, Chapman and Hall, London, UK, 1971, pp. 1–660.
- 80 C. J. O'Connor, *Prog. Inorg. Chem.*, 1982, 203–283.



ELECTRONIC SUPPLEMENTARY INFORMATION (ESI)

to

Hexanuclear $\{\text{Zn}^{\text{II}}_4\text{Fe}^{\text{III}}_2\}$ and $\{\text{Zn}^{\text{II}}_4\text{Cr}^{\text{III}}_2\}$ complexes from the use of potentially tetradentate NOO'O'' Schiff-base Ligands [†]

Konstantinos N. Pantelis ^a, Sotiris G. Skiadas ^a, Zoi G. Lada ^b, Rodolphe Clérac ^c, Yiannis Sanakis ^{*d},
Pierre Dechambenoit ^{*c}, and Spyros P. Perlepes ^{*a,b}

^a Department of Chemistry, University of Patras, Patras 26504, Greece, E-mail: perlepes@upatras.gr

^b Institute of Chemical Engineering Sciences (ICE-HT), Foundation for Research and Technology-Hellas (FORTH), Platani, P.O. Box 144, Patras 26504, Greece

^c Univ. Bordeaux, CNRS, CRPP, UMR 5031, F-33600 Pessac, France, E-mail: pierre.dechambenoit@u-bordeaux.fr

^d Institute of Nanoscience and Nanotechnology, NCSR "Demokritos", Aghia Paraskevi Attikis 15310, Greece, Email: i.sanakis@inn.demokritos.gr

[†]Dedicated to Professor Mark Turnbull on the occasion of his retirement; a great inorganic chemist and magnetochemist, a precious friend.

Table S1 Crystallographic data for complexes $[\text{Zn}_4\text{Fe}_2(\text{saphCOO})_6(\text{NO}_3)_2(\text{EtOH})_2]\cdot 4\text{CH}_2\text{Cl}_2\cdot 2\text{EtOH}$ (**1**·4CH₂Cl₂·2EtOH), $[\text{Zn}_4\text{Cr}_2(\text{saphCOO})_6(\text{NO}_3)_2(\text{H}_2\text{O})_2]\cdot 4\text{MeCN}\cdot 2\text{EtOH}$ (**2**·4MeCN·2EtOH) and $[\text{Zn}_4\text{Fe}_2(4\text{ClisaphCOO})_6(\text{NO}_3)_2(\text{EtOH})_2]\cdot 4\text{CH}_2\text{Cl}_2\cdot 2\text{EtOH}$ (**3**·4CH₂Cl₂·2EtOH)

Compound	1·4CH ₂ Cl ₂ ·2EtOH	3·4CH ₂ Cl ₂ ·2EtOH	2·4MeCN·2EtOH
Formula	C ₈₈ H ₆₆ Fe ₂ N ₈ O ₂₆ Zn ₄ · 4(CH ₂ Cl ₂)·2(C ₂ H ₆ O)	C ₈₈ H ₆₀ Cl ₆ Fe ₂ N ₈ O ₂₆ Zn ₄ · 4(CH ₂ Cl ₂)·2(C ₂ H ₆ O)	C ₈₄ H ₅₈ Cr ₂ N ₈ O ₂₆ Zn ₄ · 2(C ₂ H ₆ O)·4(C ₂ H ₃ N)
FW (g·mol⁻¹)	2456.50	2663.16	2217.21
Crystal color	brown	brown	red
Crystal size (mm)	0.24 x 0.17 x 0.10	0.09 x 0.07 x 0.02	0.11 x 0.05 x 0.03
Crystal system	monoclinic	triclinic	triclinic
Space group	P2 ₁ /c	P-1	P-1
Temperature	120 K	120 K	120 K
a (Å)	12.175(3)	12.2993(11)	12.3043(5)
b (Å)	27.856(7)	15.6707(13)	14.2093(6)
c (Å)	16.416(3)	15.6934(13)	15.7458(7)
α (°)	90	67.497(3)	109.169(2)
β (°)	113.189(15)	72.688(3)	90.594(2)
γ (°)	90	83.591(3)	113.395(2)
V (Å³)	5118(2)	2667.8(4)	2354.85(18)
Z	2	1	1
d_{calc}	1.594	1.658	1.563
μ (mm⁻¹)	1.488	1.579	1.312
θ_{min} - θ_{max}	1.462° - 23.565°	1.734° - 21.529°	1.828° - 25.091°
Refl. coll. / unique	61656 / 7381	55061 / 6132	87772 / 8353
Completeness to 2θ	0.967	0.996	0.997
R_{int}	0.1004	0.0938	0.1684
Refined param./restr.	660 / 12	681 / 18	650 / 2
^aR₁ (I > 2σ(I))	0.0791	0.0423	0.0326
^bwR₂ (all data)	0.2076	0.1099	0.0866
Goodness of fit	1.181	1.056	1.009
CCDC number	2316071	2316072	2316073

$$^a R_1 = \frac{\sum(|F_o| - |F_c|)}{\sum(|F_o|)}$$

$$^b wR_2 = \left\{ \frac{\sum[w(F_o^2 - F_c^2)^2]}{\sum[w(F_o^2)^2]} \right\}^{1/2}$$

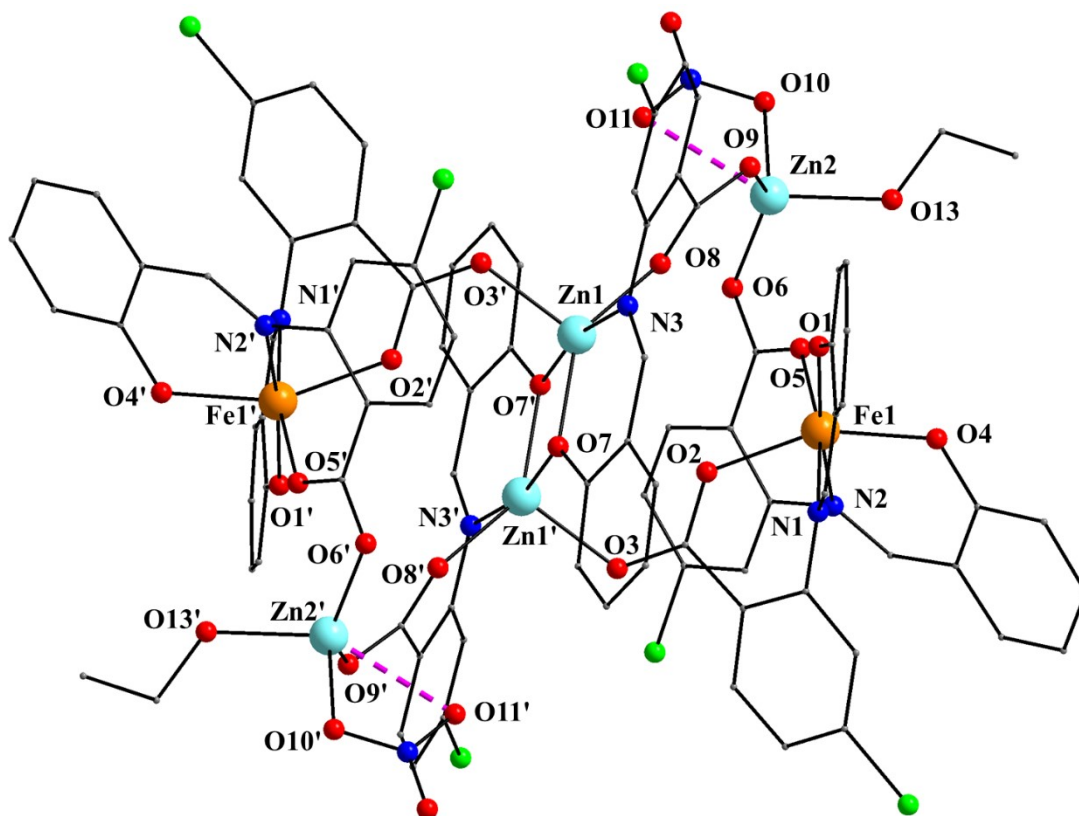


Fig. S1 Partially labeled plot of the molecule $[Zn_4Fe_2(4ClisaphCOO)_6(NO_3)_2(EtOH)_2]$ that is present in the crystal structure of $3 \cdot 4CH_2Cl_2 \cdot 2EtOH$. The dashed lines indicate a weakly bonding interaction, i.e. semicoordination. Symmetry operation used to generate equivalent atoms: (') $-x + 1, -y + 1, -z + 2$.

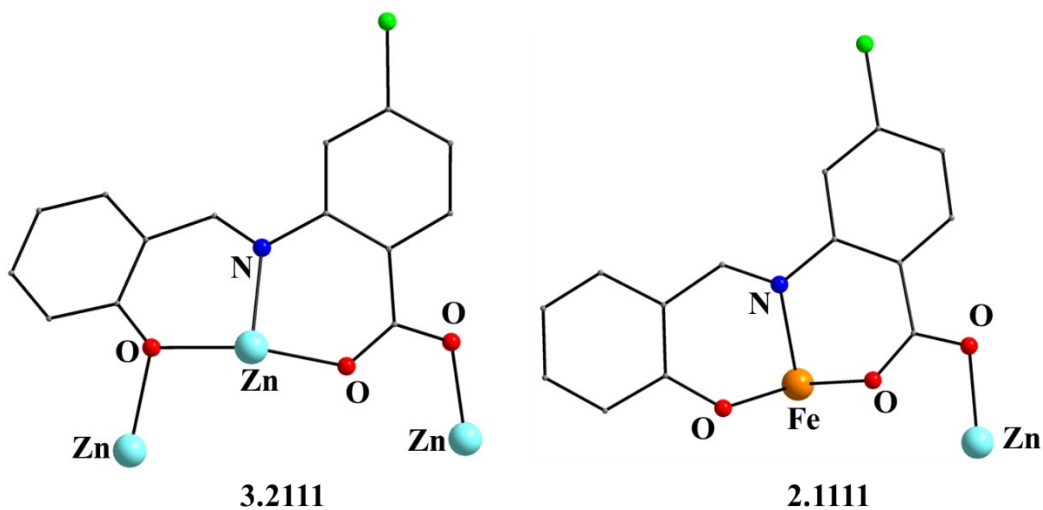


Fig. S2 The coordination modes (using Harris notation) of the $4ClisaphCOO^{2-}$ ligands in complex $3 \cdot 4CH_2Cl_2 \cdot 2EtOH$; four ligands adopt the 2.1111 ligation mode and two the 3.2111 one.

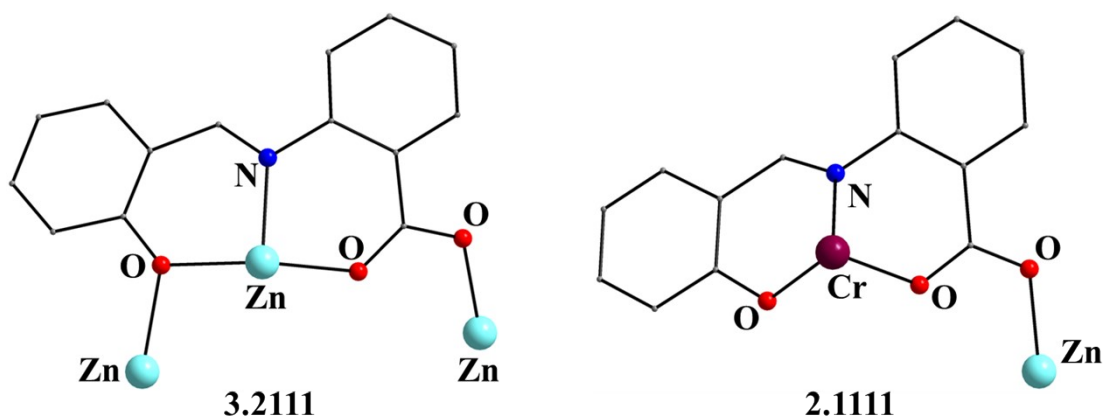


Fig. S3 The coordination modes (using Harris notation) of the saphCOO^{2-} ligands in complex $\mathbf{2}\cdot 4\text{MeCN}\cdot 2\text{EtOH}$; four ligands adopt the 2.1111 ligation mode and two the 3.2111 one.

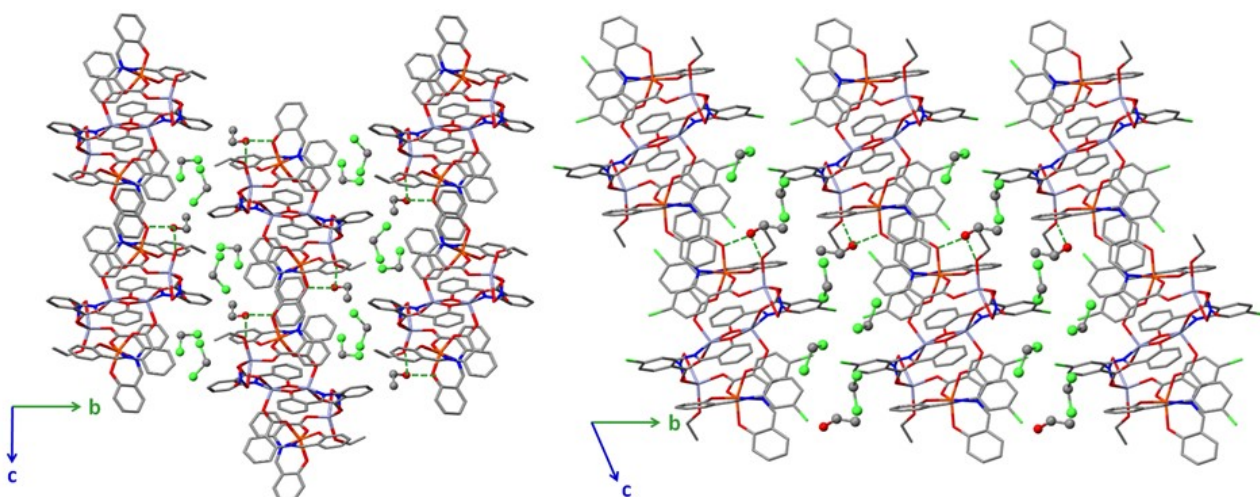


Fig. S4 Stick representations of $\mathbf{1}\cdot 4\text{CH}_2\text{Cl}_2\cdot 2\text{EtOH}$ (left) and $\mathbf{3}\cdot 4\text{CH}_2\text{Cl}_2\cdot 2\text{EtOH}$ (right) in the (bc) plane, showing the packing of the complexes separated by lattice CH_2Cl_2 molecules (depicted in ball and stick representation). H atoms are omitted for clarity. Intermolecular H bonds are illustrated with dashed green lines. C, grey; H, white; N, blue; O, red; Cl, light green; Fe, orange; Zn, light blue.

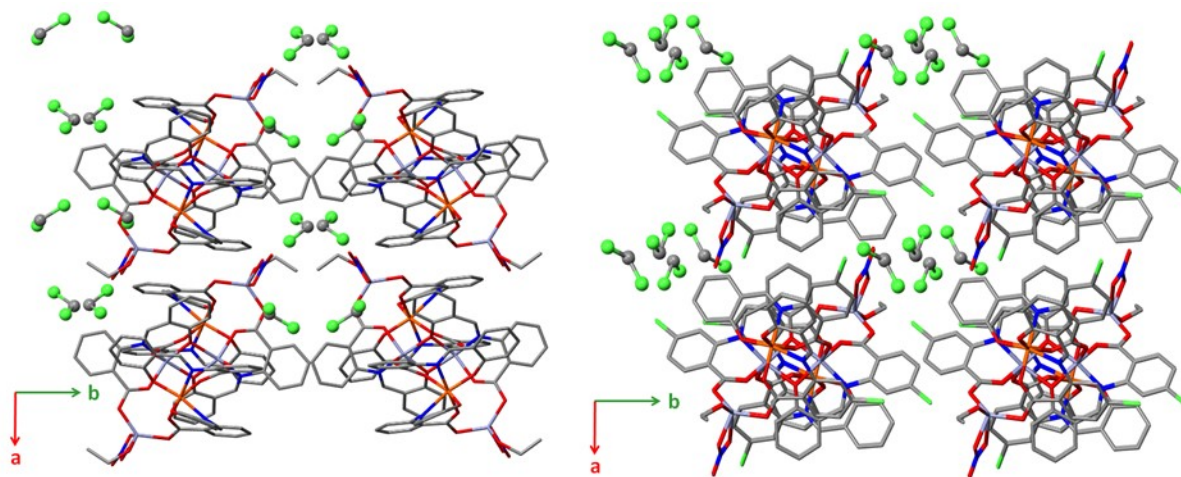


Fig. S5 Stick representations of $1 \cdot 4\text{CH}_2\text{Cl}_2 \cdot 2\text{EtOH}$ (left) and $3 \cdot 4\text{CH}_2\text{Cl}_2 \cdot 2\text{EtOH}$ (right) in the (ab) plane, showing the packing of the complexes separated by lattice CH_2Cl_2 molecules (depicted in ball and stick representation). H atoms and lattice EtOH molecules are omitted for clarity. Intermolecular H bonds are illustrated with dashed green lines. C, grey; H, white; N, blue; O, red; Cl, light green; Fe, orange; Zn, light blue.

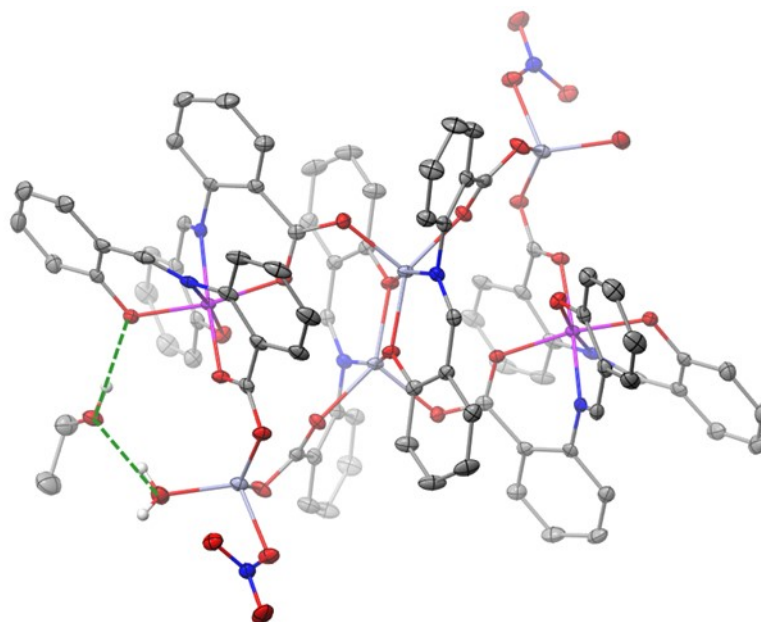


Fig. S6 ORTEP-type view of complex $2 \cdot 4\text{MeCN} \cdot 2\text{EtOH}$ and the H-bonded EtOH molecules in the crystal at 120 K. Thermal ellipsoids are depicted at a 50% probability level. Lattice MeCN molecules and H atoms are omitted for clarity, except those involved in H-bonding. H bonds are depicted in dashed green lines. C, grey; H, white; N, blue; O, red; Cr, purple; Zn, light blue.

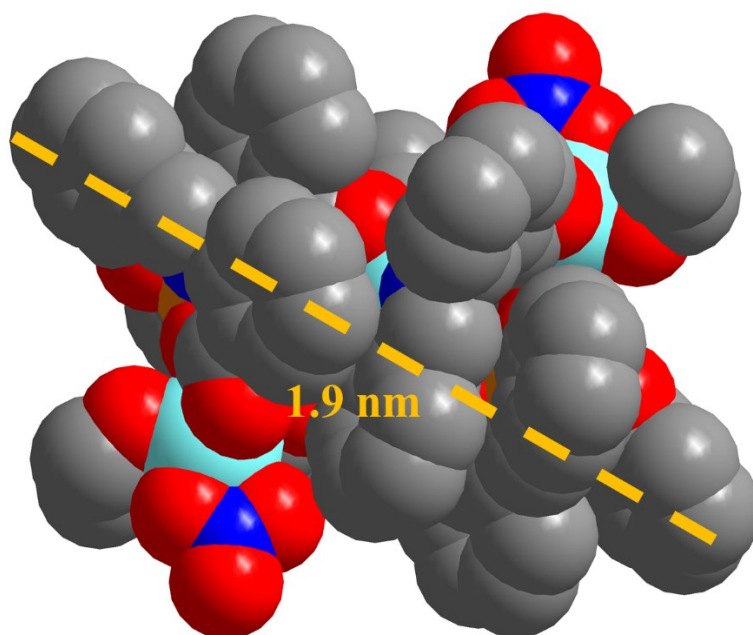


Fig. S7 Space-filling diagram of **1**.

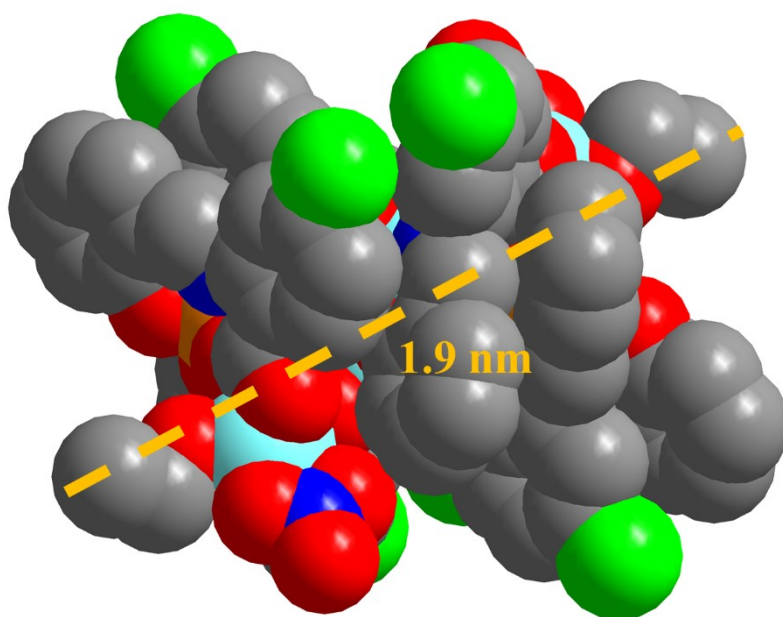


Fig. S8 Space-filling diagram of **3**.

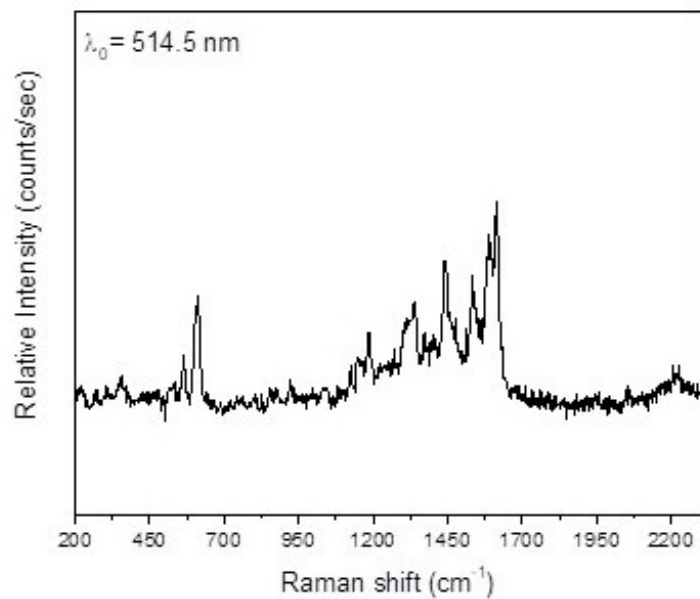


Fig. S9 The Raman spectrum of a dried sample of **1** in the 2300-200 cm⁻¹ region.

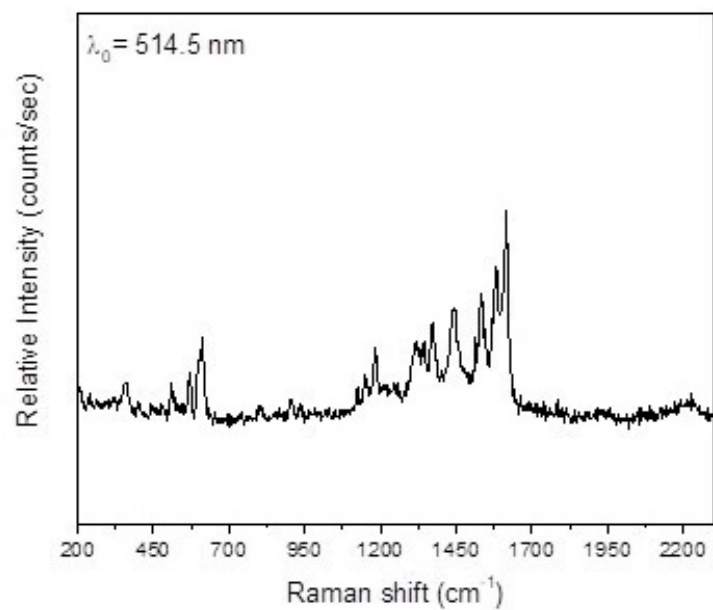


Fig. S10 The Raman spectrum of a dried sample of **3** in the 2300-200 cm⁻¹ region.

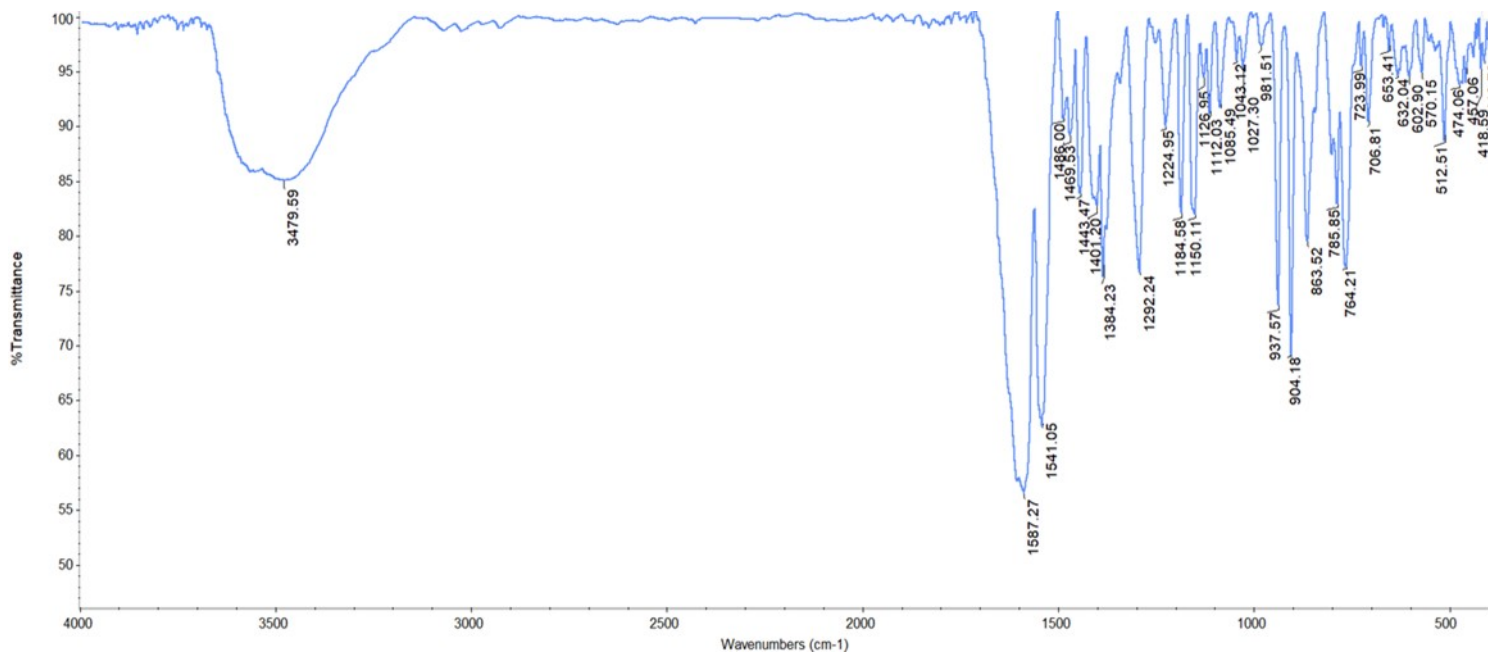


Fig. S11 The IR spectrum (KBr, cm^{-1}) of a dried sample of **3**.

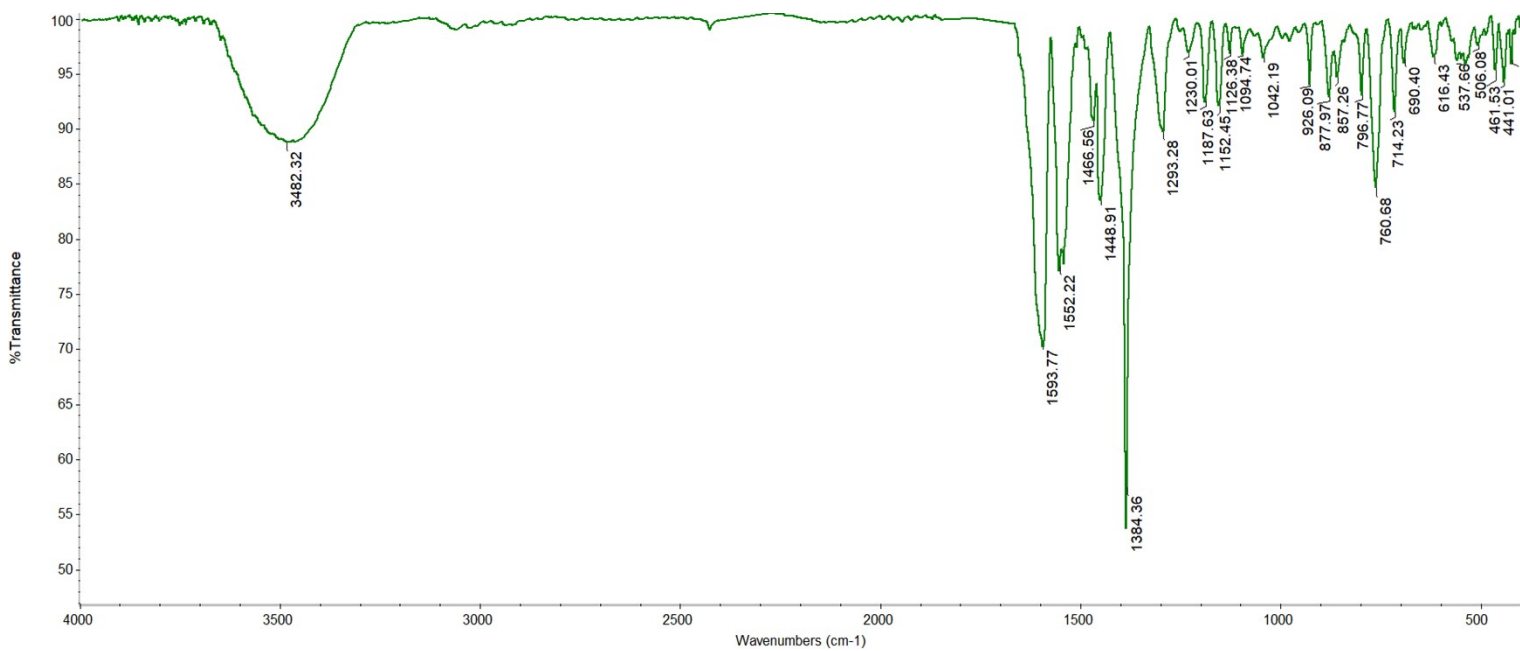


Fig. S12 The IR spectrum (KBr, cm^{-1}) of a dried sample of **2**.

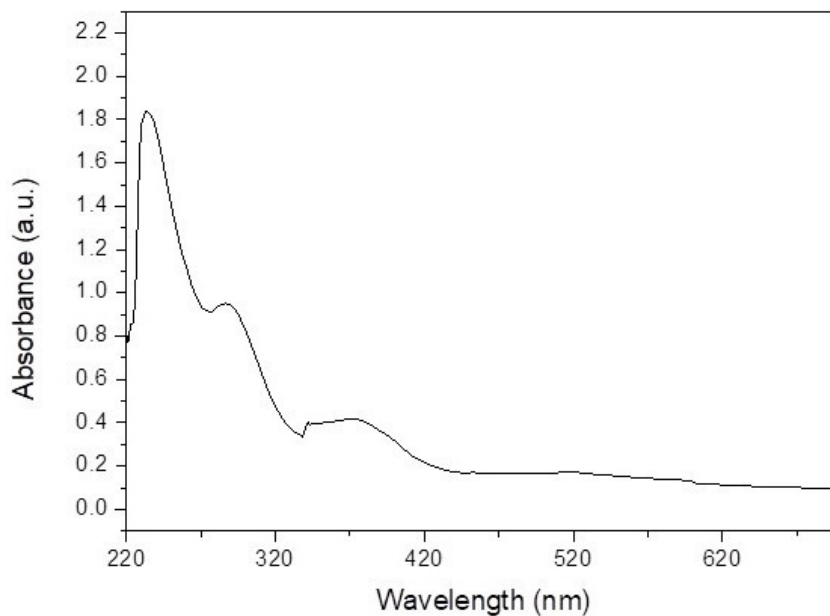


Fig. S13 The UV/Vis spectrum of a dried sample of **3** in CH_2Cl_2 . The 340 nm peak is a ghost peak due to the instrument used.

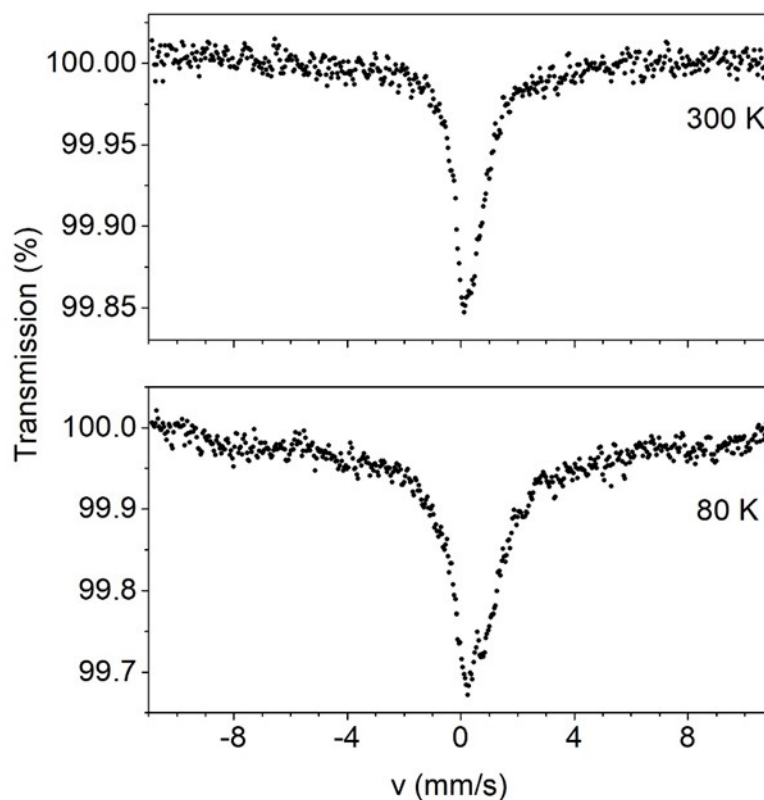


Fig. S14 Mössbauer spectra of powdered samples of complex **1** recorded at 300 and 80 K in zero applied field.

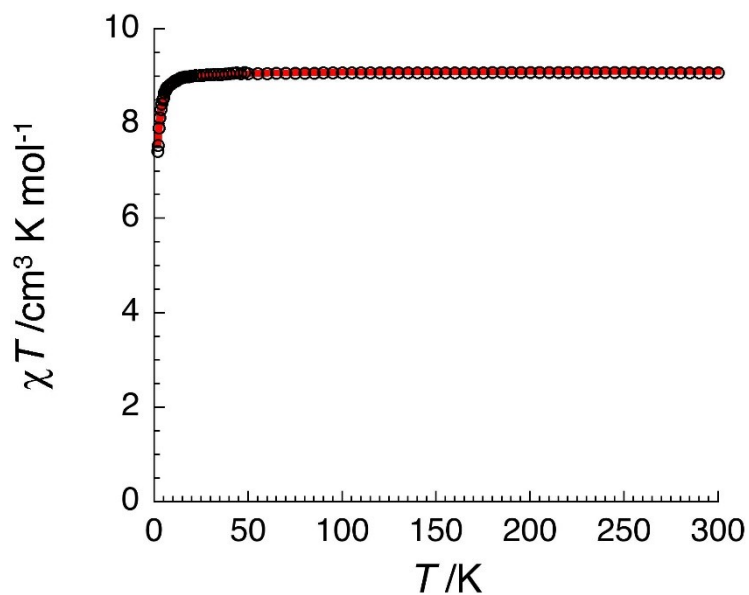


Fig. S15 Temperature dependence of the χT product (where χ is the molar magnetic susceptibility that equals M/H per complex, and T the temperature) collected in an applied dc magnetic field (H) of 0.1 T for $3 \cdot 4\text{CH}_2\text{Cl}_2 \cdot 2\text{EtOH}$. The solid red line is the best fit of the experimental data to an Heisenberg $S_{\text{Fe}} = 5/2$ spin dimer model as discussed in the text (with $\mathbf{H} = -2J(S_{\text{Fe}1} \bullet S_{\text{Fe}2})$: $J/k_B = -0.06(1)$ K and $g = 2.04(5)$).

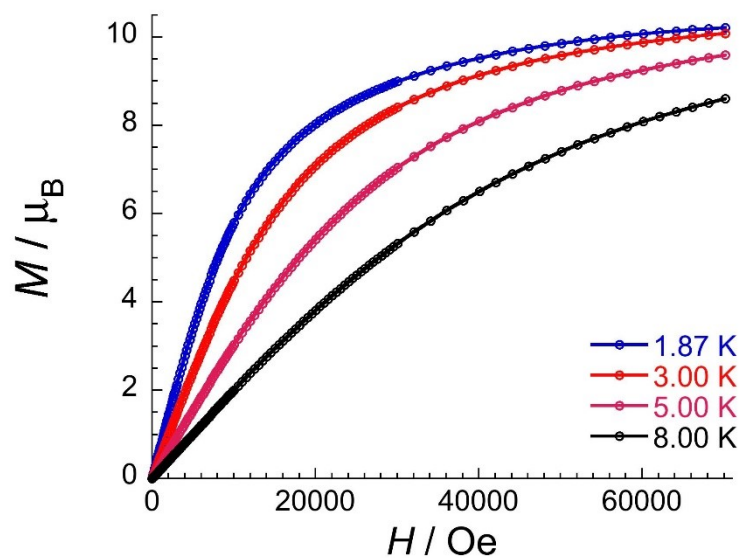


Fig. S16 Field dependence of the magnetization (M) for $3 \cdot 4\text{CH}_2\text{Cl}_2 \cdot 2\text{EtOH}$ below 8 K ($M(1.87 \text{ K}, 7 \text{ T}) = 10.2 \mu_B$ implying $g = 2.04$).

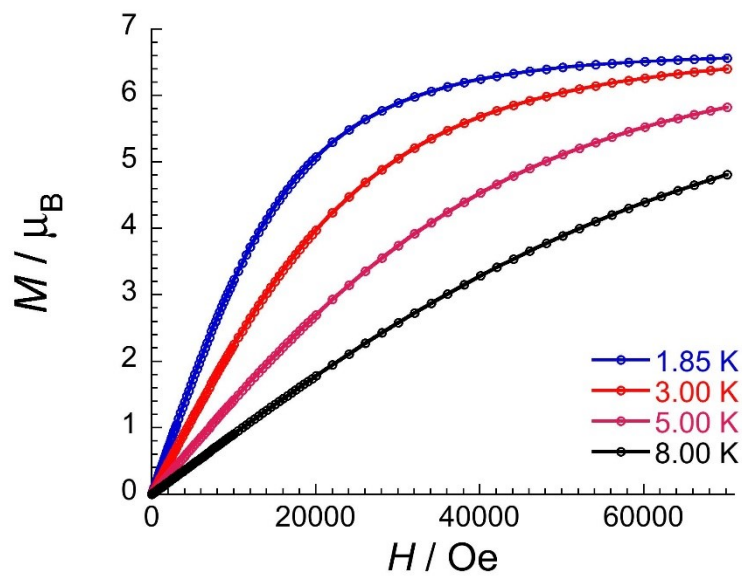


Fig. S17 Field dependence of the magnetization (M) for $2 \cdot 4\text{MeCN} \cdot 2\text{EtOH}$ below 8 K ($M(1.85 \text{ K}, 7 \text{ T}) = 6.6 \mu_B$ implying $g = 2.20$).

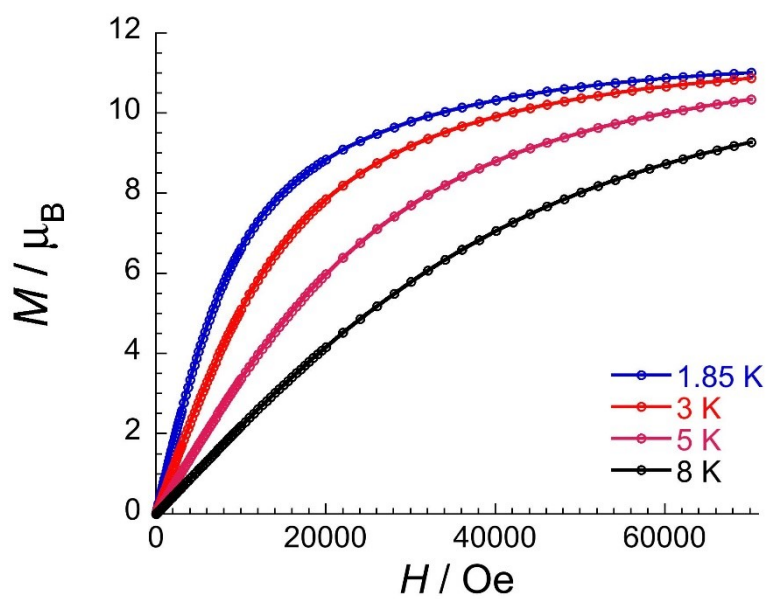


Figure S18 Field dependence of the magnetization (M) for $1 \cdot 4\text{CH}_2\text{Cl}_2 \cdot 2\text{EtOH}$ below 8 K ($M(1.85 \text{ K}, 7 \text{ T}) = 11.0 \mu_B$ implying $g = 2.10$).